Supporting Information for:

Design and Simulation of a Uniform Irradiance Photochemical Platform

Dylan J. Walsh, Timo N. Schneider, Bradley D. Olsen, and Klavs F. Jensen,

Department of Chemical Engineering Massachusetts Institute of Technology, 77 Massachusetts Avenue, Cambridge, Massachusetts 02139, United States

Table of Contents

ADDITIONAL THEORY AND DESIGN CONSIDERATIONS

When it comes to designing a lighting setup for photochemistry there are 2 general geometrical considerations: distance, and angle. The effect of light distances has two useful limits to consider: point source and area source. For a point source, the inverse square law describes how light intensity decreases at a rate of (distance, r)$^{-2}$ for a point light source (Figure 1a). [1] This result can be derived with a shell balance in spherical coordinates of light flux into and out of a control volume (Equations 1 to 5) where 'r' is the distance from light source, 'N_{light}' is the flux of light, and C is a constant.

$$In\ - Out = 0 \tag{1}$$
$$4\pi r^2 N_{light}|_r - 4\pi r^2 N_{light}|_{r+\Delta r} = 0 \tag{2}$$
$$\lim_{\Delta r \to 0} \frac{r^2 N_{light}|_r - r^2 N_{light}|_{r+\Delta r}}{\Delta r} = 0 \tag{3}$$
$$\frac{d}{dr}\left(r^2 N_{light}\right) = 0 \tag{4}$$
$$N_{light}(r) = \frac{C}{r^2} \tag{5}$$

The origin of this is the increased surface area that the light is casted on with changes in distance. For an area source with light emitted purely normal to the surface, the light intensity remains constant with changes of distance. The inverse square law applies well (less than 1% error) when the light source radius is x10 smaller than distance to the surface, and the area source situation applies well when the light source radius is x10 larger than the distance to the surface.[2] Together these two situations place limits on what can be expected as light intensity varies with distance; however, typical photochemical experimental setups fall in between these limits (0.1< distance/light source radius < 10) (see Figure 15). The second geometrical consideration relates to the cosine law, which states that the light intensity through a surface is proportional to the cosine of the angle in which the light hits the surfaces (Figure 1b).[1] Trigonometry provides the derivation (Equations 6 to 7) with A_i being the surface 'i', θ being the angle of incidence and N_{light,A_i} being the flux of light through the area 'A_i'.

$$A_1 = \frac{A_2}{\cos(\theta)} \tag{6}$$
$$N_{light,A_1} = N_{light,A_2}\ cos(\theta) \tag{7}$$

The origin of this is the increase in surface area that the light is cast on with changes in angle of illumination. For a point source over a flat surface, these effects combine to produce a high intensity of illumination directly under the center of the light, but the intensity falls off rapidly with distance from the origin (Figure 1c). To get an analytical solution, Equations 5 can be combined with Equation 7, converted to cartesian coordinates (x, y, z), and evaluated at z='h', the height of the light above the surface to yield Equation 10.

$$r^2 = x^2 + y^2 + z^2 \tag{8}$$

$$cos(\theta) = \frac{z}{\sqrt{x^2 + y^2 + z^2}} \tag{9}$$

$$N_{light}(x,\ y)|_{z=h} = \frac{C}{x^2 + y^2 + h^2}\left(\frac{h}{\sqrt{x^2 + y^2 + h^2}}\right) \tag{10}$$

Together the distance and angle of a light source from the surface combine to dramatically affect the level of irradiance and its uniformity.

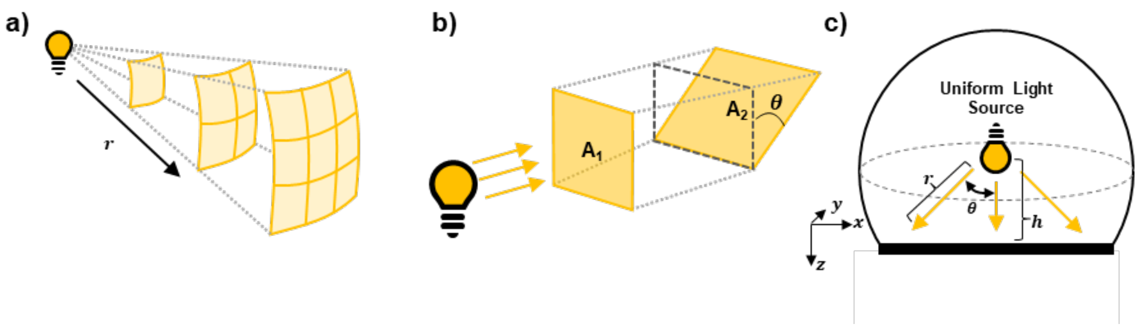

Figure 1: Geometrical considerations of light placement. a) Inverse-square law: light decreases intensity at a rate of radius squared. b) Cosine law: flux of light through an angle surface is decrease by the cosine of the angle normal to the light. c) Effects of inverse square law and cosine law on a flat surface.

On top of the general geometrical effects, the light source radiance profile can affect illumination intensity and uniformity.[3–6] LEDs typically do not have uniform radiance profiles and tend to bias light generation toward the center which can increase intensity of light in the direction the LED is pointing. At mid to far distances (distance/light source radius>5), LEDs can typically be approximated to be a Lambert cosine emitter, similar to the cosine law, where the emissions from the light source are directly proportional to the cosine of the angle from normal.[4–6] Manufacturers typically provide the emission profiles in datasheets along with their product as the emission profiles can vary greatly across series, type, lens, etc. One import caveat is that the emission profiles characterized in manufacturers data sheets are typically a far distance emission profile, which are not representative of emission profiles at short distances (distance/light source radius<5) where LEDs are often placed for photochemistry.[6] In this case, the point source approximation breaks down leading to deviations in the emission profile. As a result, photochemical setup designs may need to change depending on the exact type of LED used.

RAY TRACING ALGORITHM AND CODE

To setup a ray tracing simulation, the lights and surfaces need to be defined. To define a light, the light's position (x, y, z), direction (x, y, z), emission profile (broken into phi and theta components of a spherical coordinate system), and number of rays must be provided. The default emission profile is of a uniform point source which can be exchanged for any real-world light profile that a user provides. Area light sources can be modeled by arrays of point sources. To define a surface, the surface's position (x, y, z,), normal vector (x, y, z), length, width, and transmission type must be provided. The transmission type is typically 'absorb' to signify that any rays that hit the surface are purely absorbed (vs. reflected or transmitted), however it can also be set to 'reflect' or 'transmit'. In the case where the transmission type is set to 'reflect', the surface would act as a mirror. Typical low-cost mirrors reflect 70-90% of the light which can be specified with a probability of reflection function (vs. absorption).[7] If the transmission type is set to 'transmit', the surface can act as a diffuser. The diffuser's behavior can be defined by providing a probability of transmitting and a scattering emission profile to specify how the transmitted light path changes after passing through the surface. With the lights and surfaces defined, the last parameter to setup the simulation is the maximum number of bounces (reflections/scattering) a ray can have. If there are only 'absorbing' surfaces in the simulation, this can be set to zero for fast computations, however if there are any surfaces that 'reflect' or 'transmit', then it should be set to a value larger than 1.

With the lights and surfaces defined, the model performs the ray tracing computations by casting rays of light from the light sources and tracing their path through the 3-dimensional simulation until they are absorbed. The first step of the calculations is to generate rays for each light. To generate rays, a set of random numbers [0, 1] are generated equal to the number of desired rays. This randomly generated set of numbers is used to produce phi values between [0, 2*pi]. Another set of random numbers are generated for the theta component and redistributed to account for the change in surface area of a differential element of a solid angle.[8] With the phi and theta components, the rays can be converted to cartesian unit vectors and rotated to the direction vector of the light source with quaternion. Following the generation of rays, the raytracing occurs by calculating dot product between a surface's normal vector and the ray's direction vector to see if the ray is pointing toward the surface. If the ray does point at the surface, then the direction in which the ray hits the surfaces is calculated (determine if the ray hits the top or bottom of the surface) with the dot product of the surface's normal vector and the vector that goes between the ray's position to the surface's position. If the ray is hitting the surface and is going through the top side, the intersection point can be calculated and compared to see if it is within the bounds of the surface. This calculation is performed on every ray with every surface until a valid intersection is found, otherwise the ray did not hit any surfaces in the simulation and can be disregarded from further calculation. If the intersection occurred on an absorbing surface, the location of intersection is noted, and the ray tracing process stops for that ray. If the intersection occurred on a reflecting surface, the probability of reflecting is calculated with a random number generator, and if it does not reflect, then it is treated as an absorbed ray on that surface otherwise we calculate the reflected vector. If the intersection occurred on a transmitting surface, the probability of transmitting is calculated with a random number generator, and if it does not transmit it is treated as an absorbed ray or reflected ray. If it does transmit, then the transmitted ray is calculated in a similar mechanism as the rays generated from a light source, with the difference being that the angle of the incoming ray into the surface becomes the direction vector for the new ray and the emission profile is based off a user provided function. Raytracing continues till all rays have been absorbed or the max bounce limit has been reached.

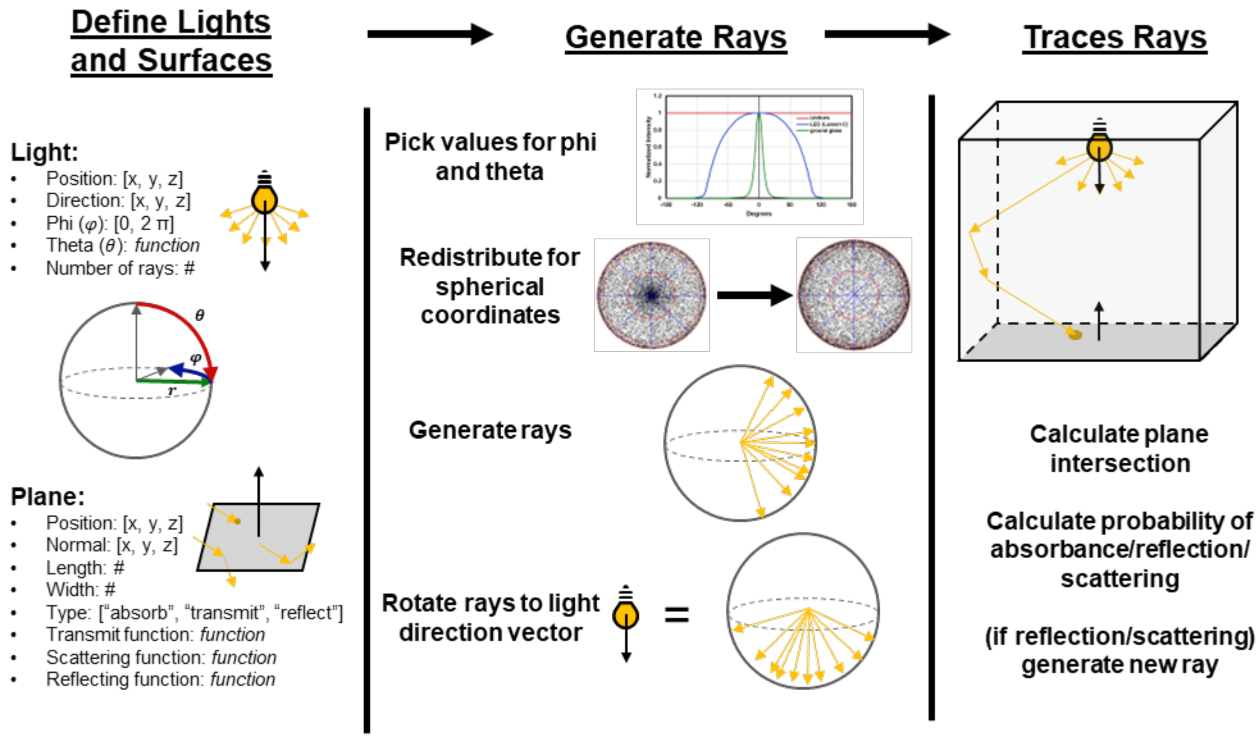

Figure 2: Overview of simulation process. The simulation begins with defining the lights and surfaces. This is followed by generating the rays, and finishes with tracing the rays to their final location.

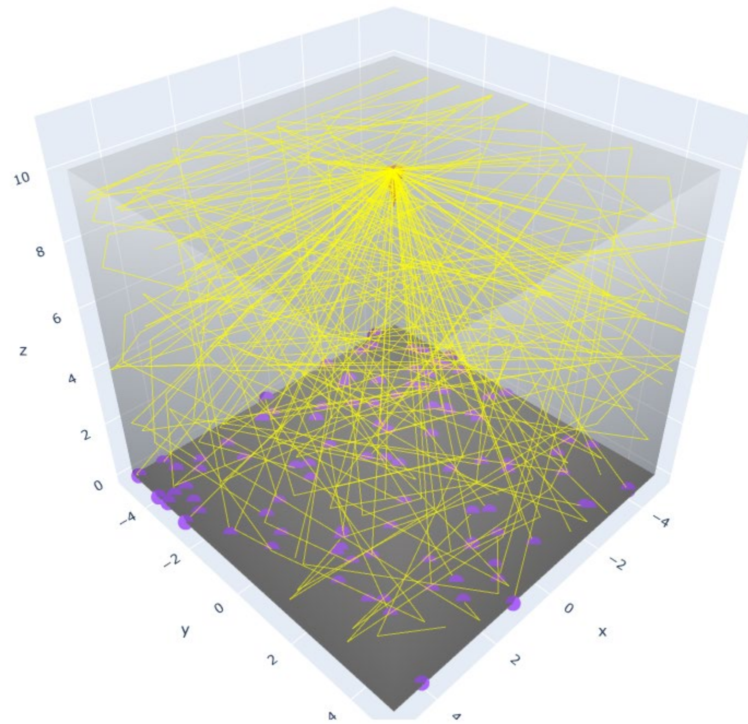

Figure 3: 3D plot of ray traces (yellow lines) for a single point source (orange cone at [0, 0, 10]) in a mirror box of dimensions 10 x 10 x 10 with an absorbing ground plane. purple circles: absorbed rays on the ground plane.

Code

All code for running the simulation and generating data, figures, etc. can be found:
https://github.com/dylanwal/raytracepy
version: 0.0.1

The simulation has been packaged for pip installation 'pip install raytracepy'.
pip website: https://pypi.org/project/raytracepy/0.0.1/

VALIDATION OF RAY TRACING CODE

Inverse Square Law

For the inverse square law, a series of simulations with a uniform light source at different distances ranging from 1 cm to 10 cm above a flat absorbing surface. The light intensity at the center of the surface was then calculated for each height of the light source. Specifically, the hits within a 0.1 mm circle around point (0, 0) were used as an equivalent to light intensity. The data was normalized (with respect to the value at 10 cm), plotted on a ln-ln plot, and a line was fit to determine the slope (Figure 4). The results show that the data has a perfect inverse square dependence with respect to light height matching theory.

The experimental data for the inverse square law was collected using an iPhone 5 SE camera light as the light source. The phone's light was placed directly centered over the radiometer, and the distance between the phone and the radiometer sensor was measured and a spectrum was collected. The phone was moved to another height and another spectra was collected. This process repeated to collected data over a range of 3.5 cm to 12 cm.

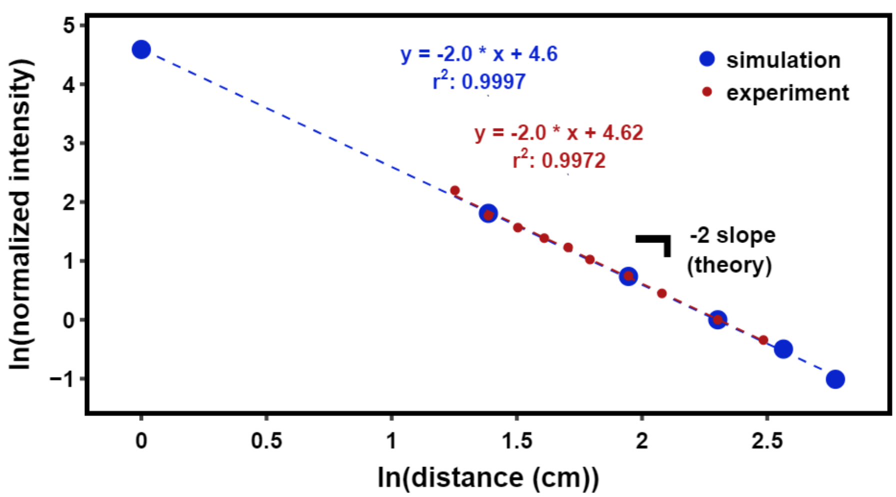

Figure 4: Plot of theory, simulation, and experimental data for the inverse square law. The x-axis distance is the distance between the light source and detector.

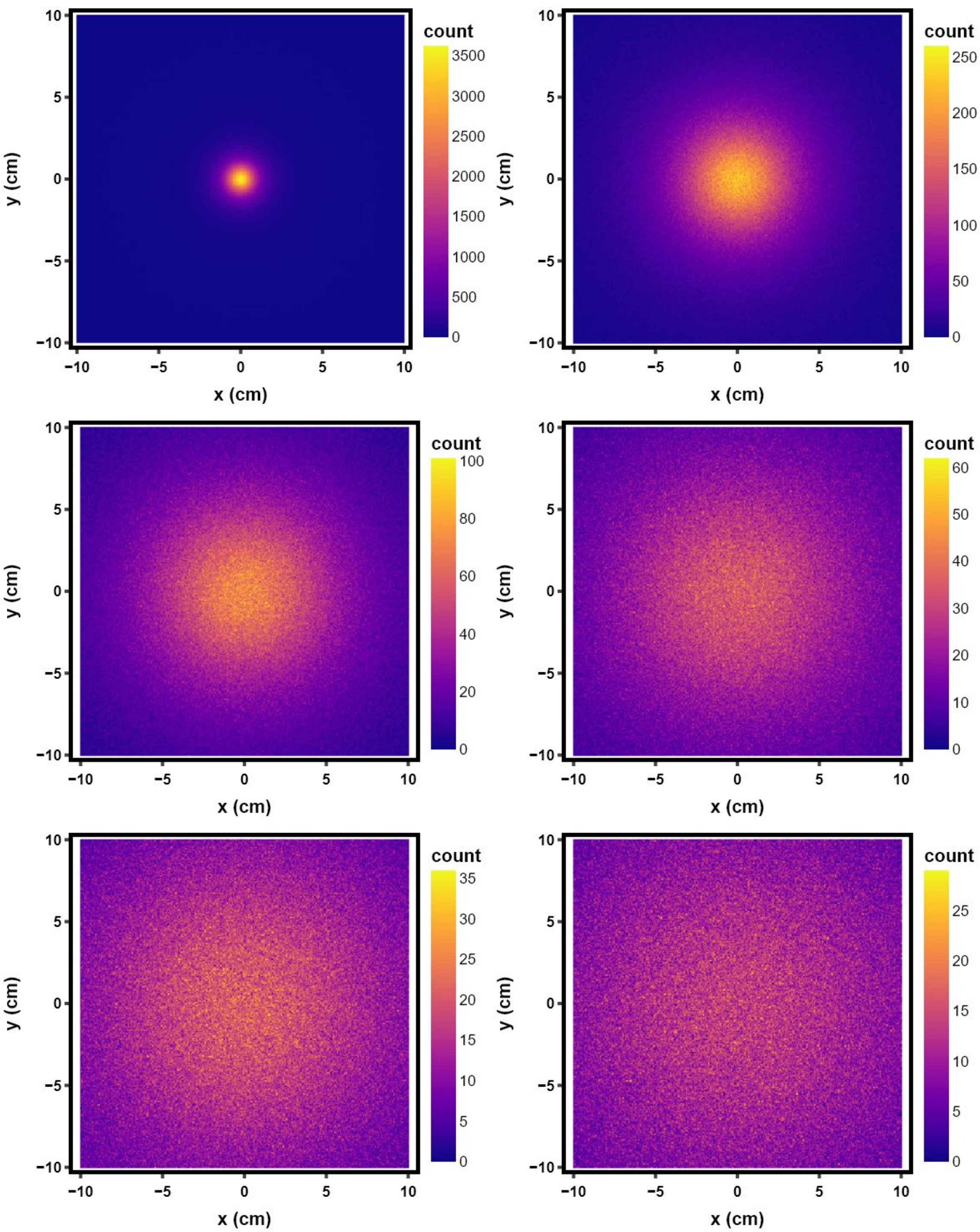

Figure 5: 2d histogram of hits on a flat surface from a single point light source at various heights above the surface.

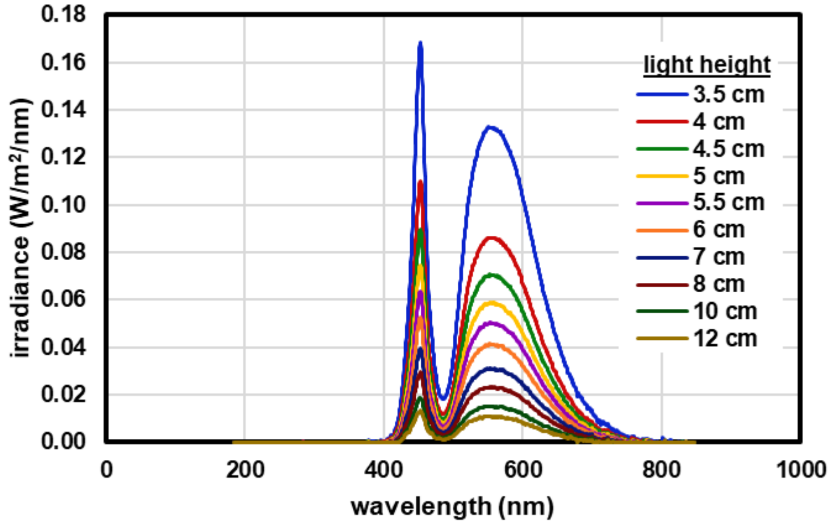

Figure 6: Radiographs for the inverse square law.

Cosine Law

For the cosine law, we setup a series of simulations with a uniform light source at a radius of 5 cm from the center of a flat surfaces which was placed at various angles ranging from 0 (perfectly normal to the surface) to $\pi/2$ (in line with the surface). Once again, we calculated how the light intensity at the center of the surface changes as the angle of the light source changes. Specifically, the hits within a 0.1 mm circle around point (0, 0) were used as an equivalent to light intensity. The data was normalized (angle = 0 rad was set to 1), plotted, and compared against the cosine function (Figure 7). The results show a near perfect agreement with the cosine law.

The experimental data for the inverse square law was collected using an iphone 5 SE camera light as the light source. A string was attached between the phone and the radiometer to ensure that the distance between remained constant at 10 cm. The light was then placed at various angles with 0 rad corresponding to directly above the radiometer.

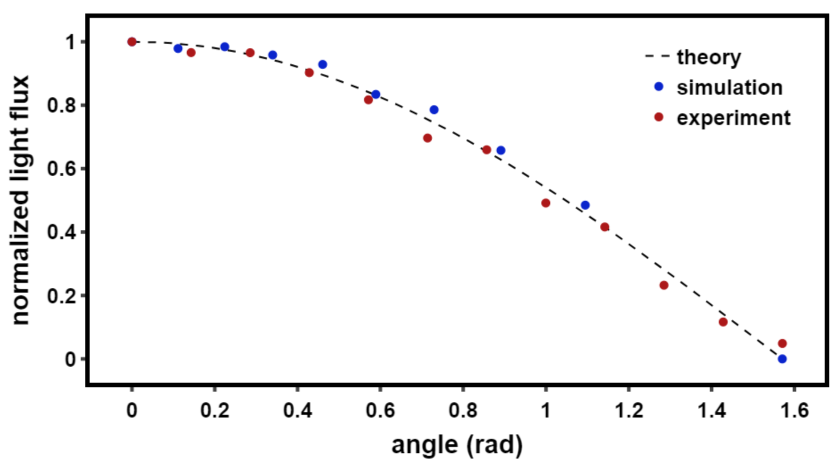

Figure 7: Plot of theory, simulation, and experimental data for the cosine law. The x-axis angle is relative to the normal vector of the detector.

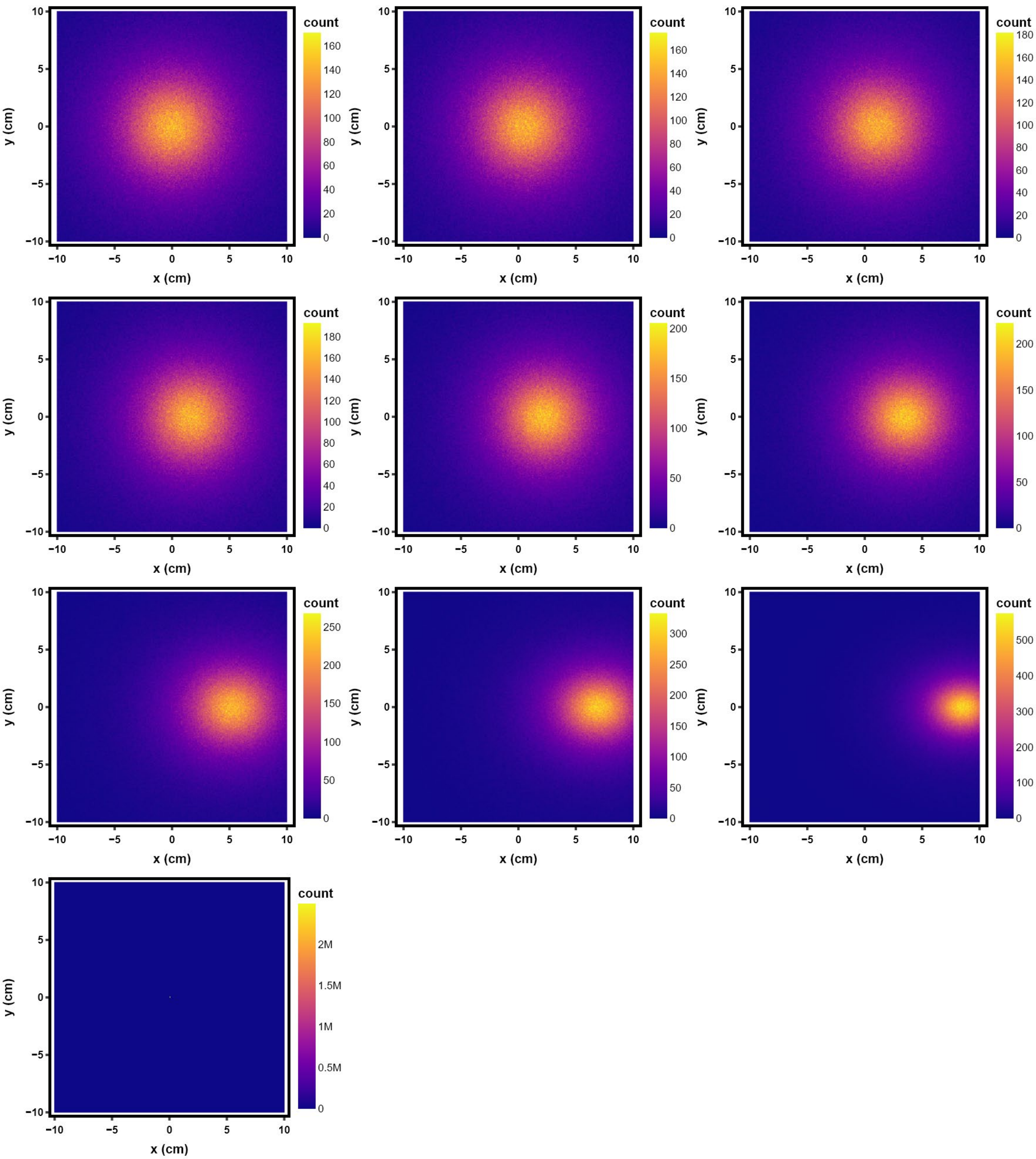

Figure 8: 2d histogram of hits on a flat surface from a single point light source at various angles off the surface.

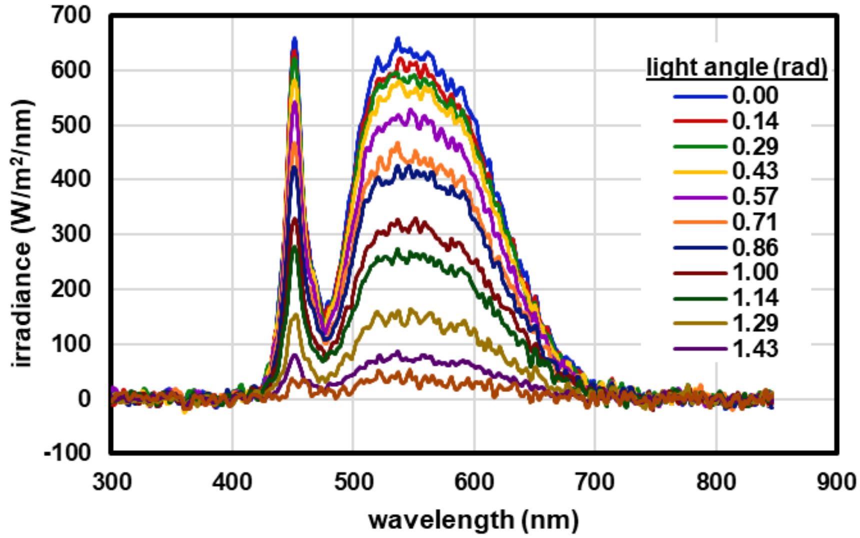

Figure 9: Radiographs for the cosine law.

Point Source on Flat Surface

The third validation we looked at was to compare the light intensity profile on a flat surface to the theoretical derivation found in Figure 1c. Using the same simulation results calculated from the inverse square law, the simulation perfectly reproduces the theoretical profiles calculated using the equation in Figure 1c (Figure 10).

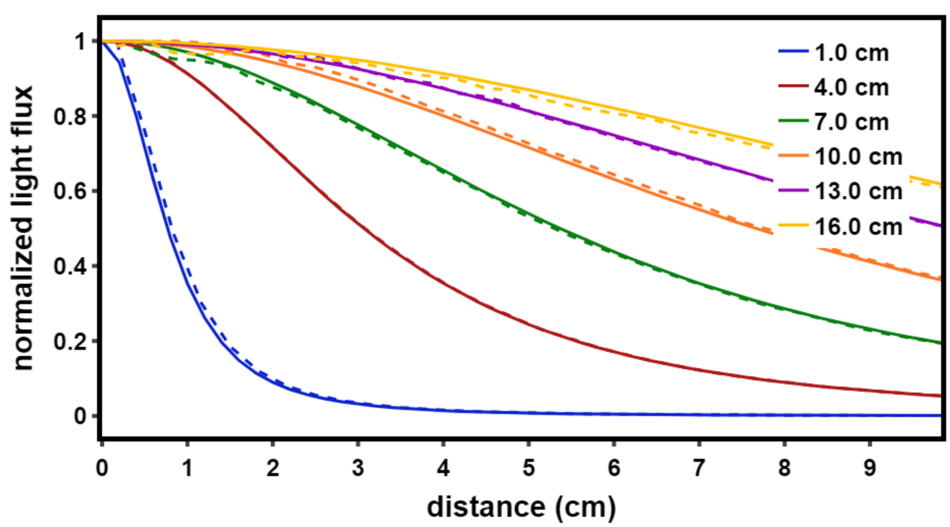

Figure 10: Plot of radial distribution function for irradiance vs distance from the center of a flat surface for simulation (solid lines) and theory, equation 10 (dashed lines).

Rays Need Per Simulation

To determine the number of rays, need for a simulation for it not to have significant statistical error, a series of simulations with a uniform light source with a different number of rays ranging from 10,000 to 5,000,000. The uniform light source was place 4 cm above a flat absorbing surface, 20 cm by 20 cm. The light intensity was radial averaged and compared to theory (equation 10). Based on the data in Figure 11 and Figure 12, the use of >100,000 rays are needed to get a good match to theory. Note that this will change per situation, and this is just to give a rough prospective of a valid number of rays. In general, we used 5 million rays to be well within the valid numerical results region, and to keep the simulation time to under a minute.

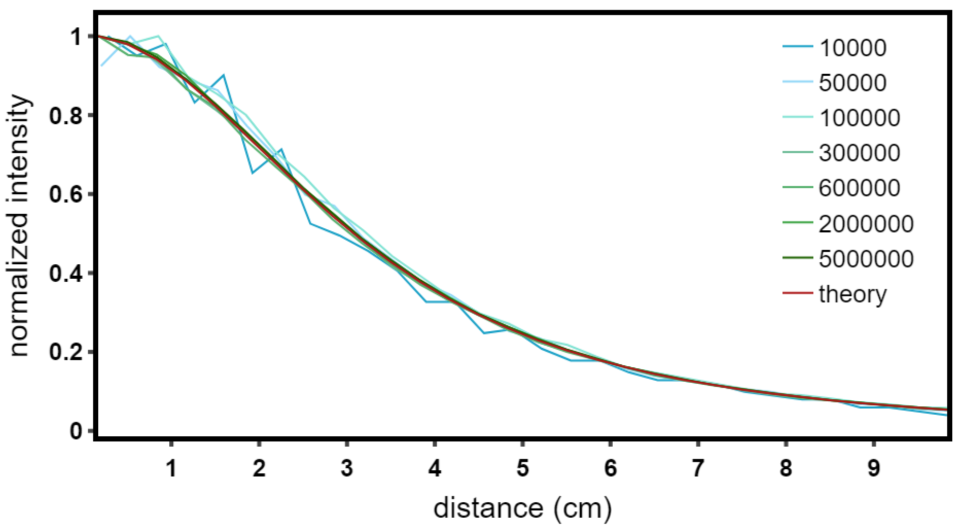

Figure 11: Plot of radial distribution function for normalize intensity vs. distance from the center of a flat surface with different number of rays used in each simulation. The legend numbers are number of rays used in the simulation. Theory is from equation 10 (dashed lines).

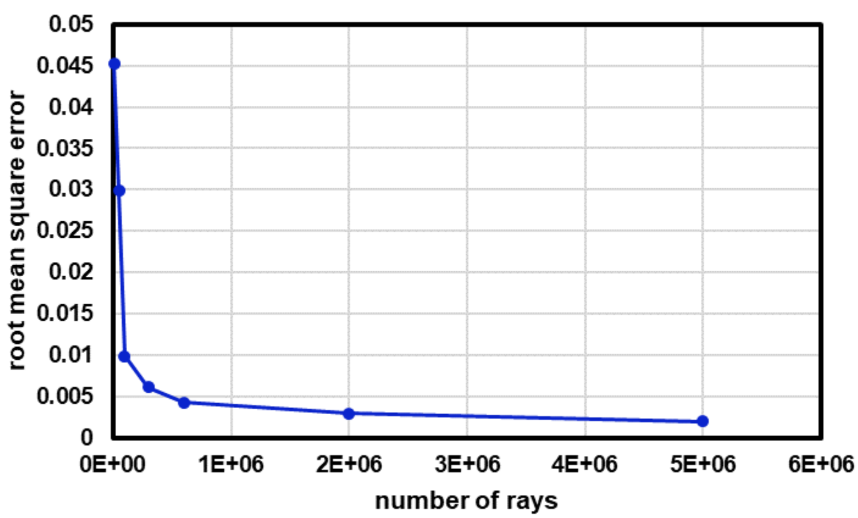

Figure 12: Root mean squared difference between theory and simulation (with different number of rays) for the radial distribution function.

Reflection

To validate the ray tracing simulation for non-uniform light sources, the analytical expression in Figure 1c can be modified, leading to :

$$N_{light}(x, y)\,|_{z=h} = \frac{C(\theta)}{x^2 + y^2 + h^2}\left(\frac{h}{\sqrt{x^2 + y^2 + h^2}}\right) \tag{11}$$

$$\theta = \arccos\left(\frac{h}{\sqrt{x^2 + y^2 + h^2}}\right) \tag{12}$$

The radiant intensity of the emitter at the source $C(\theta)$ depends now, in contrast to the uniform model, on emission angle. Further dependencies on specific direction at a fixed emission angle are neglected. The radiant intensity profile found in the datasheet of the LEDs (see 'Emission and Transmittance Profiles' for details) is fit using a polynomial resulting in the continuous function $C(\theta)$. This analytical solution can further be expanded for mirror on all sides of the setup to validate the reflection aspect of the ray tracing algorithm. The light flux at a point on the surface is found by summing up the light fluxes of mirror images of the original surface which are weighted with decreasing values to account for the mirror's reflection efficiency (Figure 13). Each light beam going to a red point in this new plane will end up after a certain number of reflections *R* on the original red point. Therefore, the final irradiance at the position of interest is given by the sum of all those irradiance values, after accounting for mirror efficiency *E*. Up to 50 reflections are considered.

$$N_{mirr}(x, y)\,|_{z=h} = \sum_i N_{light}(x_i, y_i)\,|_{z=h} * E^{R_i} \tag{13}$$

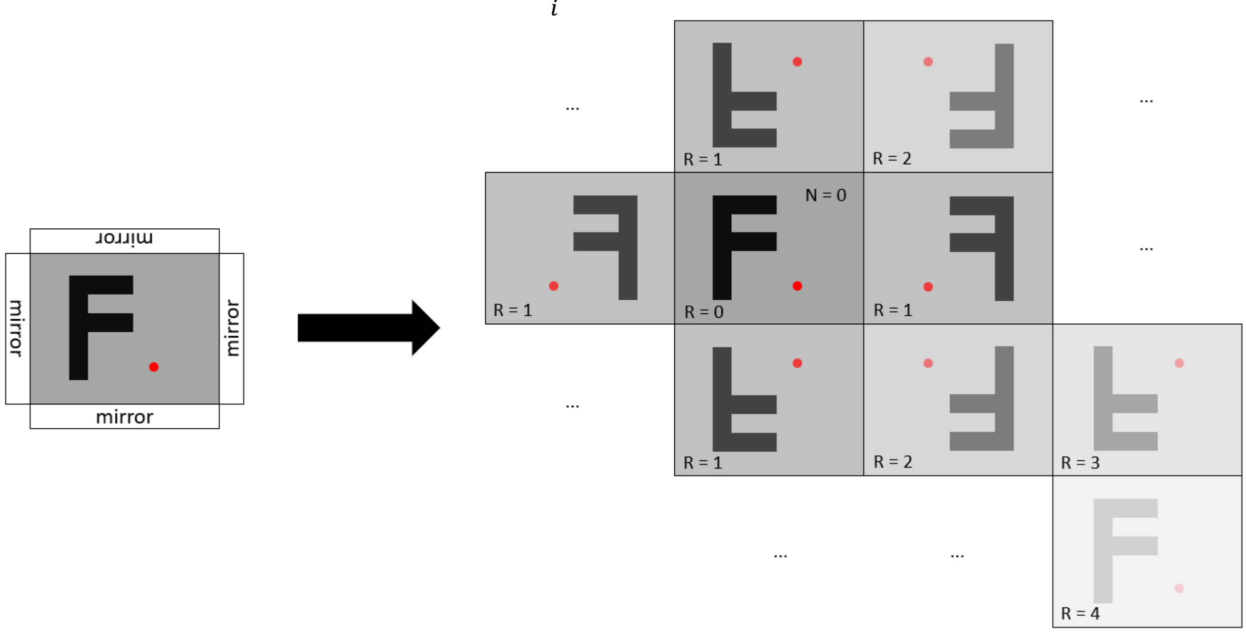

Figure 13: Conceptual diagram for modeling reflection of a mirror box by considering the irradiance values of mirror images of the original surface. The square 'R=0' is the surface we which to compute the irradiance of. The squares for R=# correspond to the number of reflections away from the target plane that square is.

Comparing the ray tracing algorithm to the analytical solution, heat maps of irradiance for a single LED light source 5 cm above a 10 cm x 10 cm absorbing surface surrounded on all 4 sided by mirrors with an 85 % efficiency we calculated (Figure 14). Visually, the heat maps look identical, and a quantitative analysis can be done by comparing the percentiles between the two heatmaps (2d histograms). The percentiles are nearly identical demonstrating that the raytracing model accurately predicts reflections at mirror surfaces and non-uniform light sources.

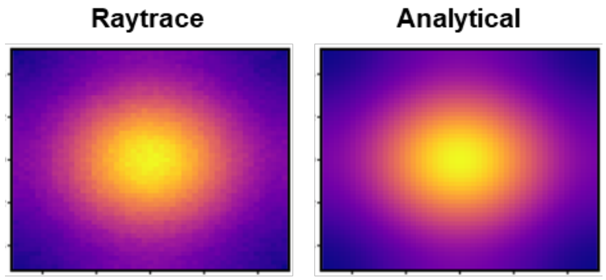

	Min	p10	p30	p70	p90	Max
Raytrace	0.716	0.802	0.885	1.06	1.28	1.46
Analytical	0.757	0.815	0.892	1.06	1.27	1.43

Figure 14: Normalized irradiance heat maps of a single LED light source 5 cm above a 10 cm x 10 cm absorbing surfaces which is surrounded on all 4 sided by mirrors with an 85 % efficiency. The heat map on the left was produced by the raytracing algorithm, and the heat map on the left was produced by the analytical approach. The results are compared by providing a table of normalized irradiance percentiles, i.e. ‘p10’ is the irradiance value at the 10th percentile of the heat map.

RAY TRACING ANALYSIS

Figure inspired by reference.[2]

$$N_{light} = Light\ intensity$$
$$r = radius\ of\ light\ source$$
$$d = distance\ from\ light\ source$$

Area light source:

$$N_{light} = constant \tag{14}$$

Circular light source:

$$N_{light} = \frac{r^2}{r^2 + d^2} \tag{15}$$

Point light source:

$$N_{light} = \frac{1}{d^2} \tag{16}$$

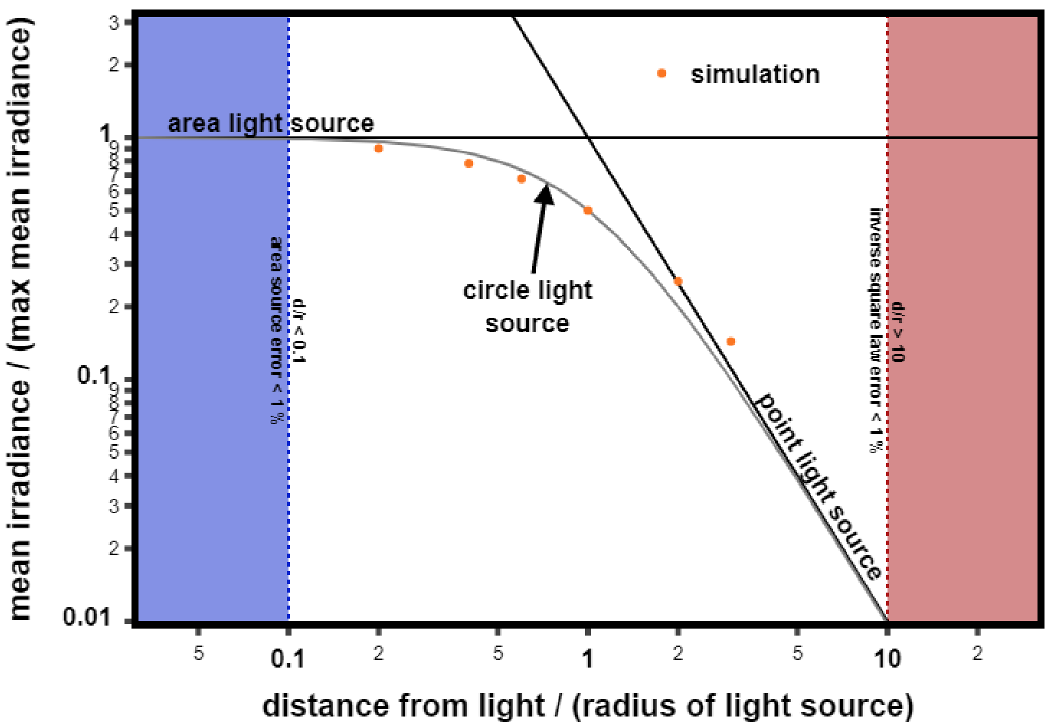

Figure 15: Plot of mean irradiance vs distance from light for various regimes. Simulation data from figure 3c of the main manuscript is added as well.*

* It is hard to define what a radius means for a square light source, so a radius of 5 cm was used as an approximation for the 10 cm x 10 cm light array.

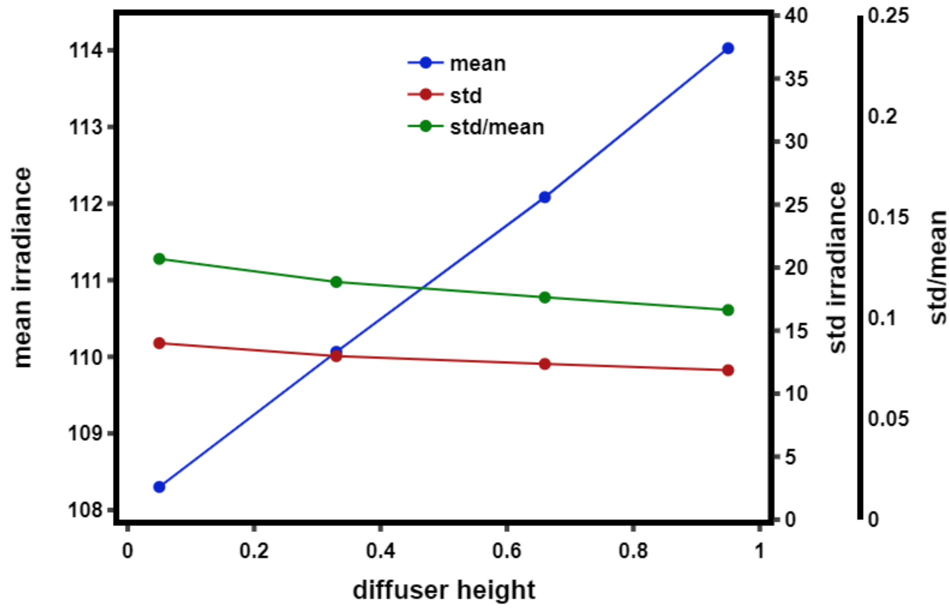

Figure 16: Dependence of mean and std on the relative distance between of the diffusing surface for the offset grid light pattern at a light height of 5 cm and with a pattern width of 12.5 cm. (diffuser height: 0 = surface, 1 = light height)

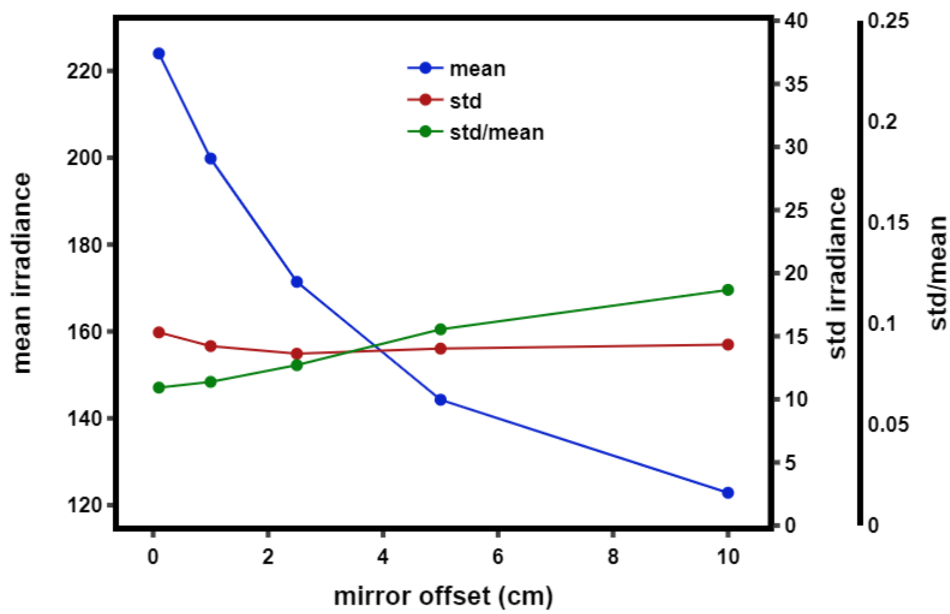

Figure 17: Dependence of mean and std on the distance between the mirrors and outermost lights for the offset grid light pattern at a light height of 5 cm and with a pattern width of 12.5 cm.

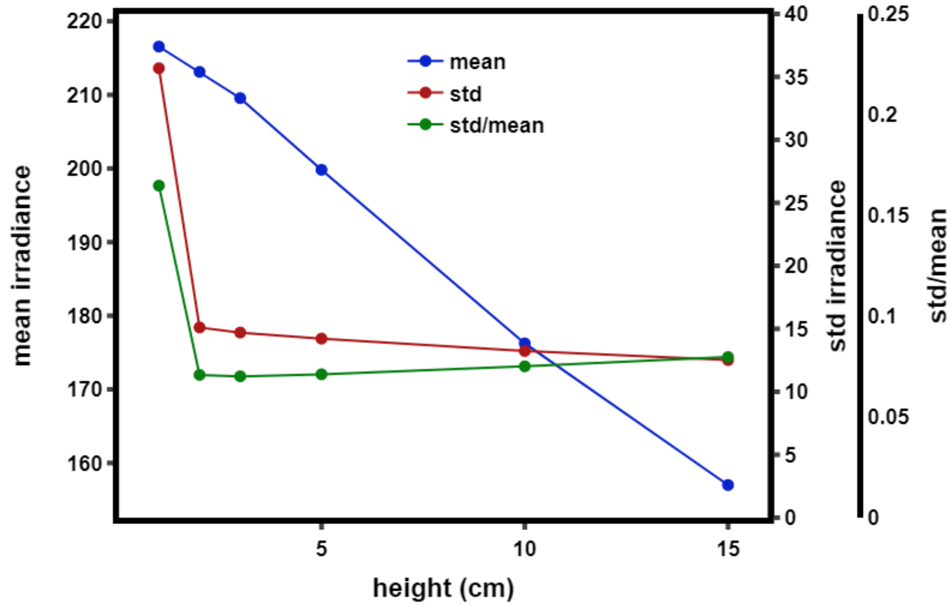

Figure 18: Dependence of mean and std on the height of lights for the offset grid light pattern with a width of 12.5 cm and mirror offset of 1 cm.

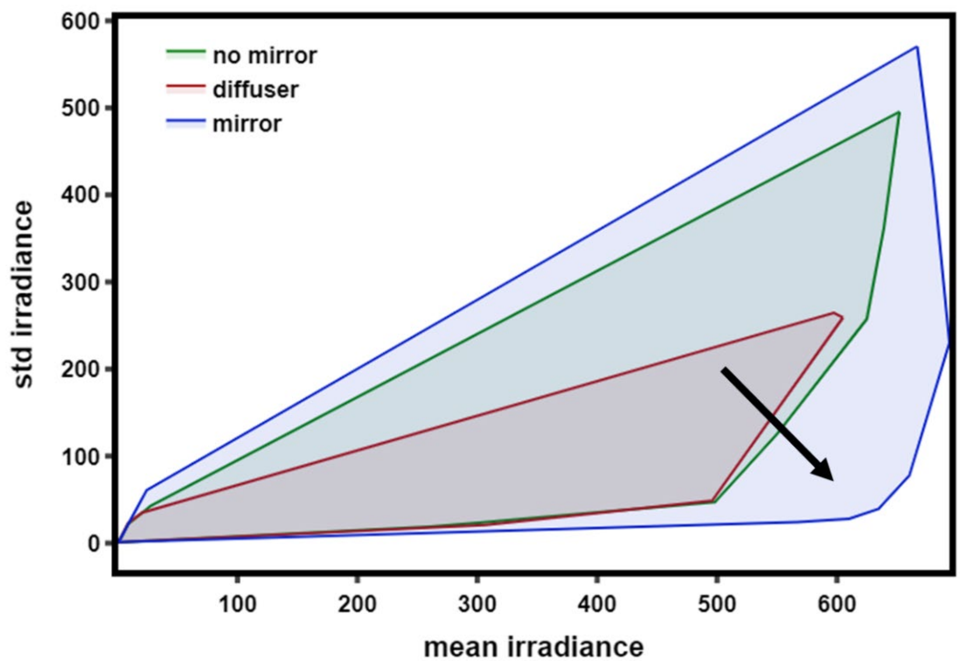

Figure 19: Convex hull for the offset light grid with and without diffusor or mirrors in the mean/std irradiance space. The arrow indicates the region that is most beneficial (high uniformity and light intensity) for the convex hull to expand into. (Full version of Figure 5 from the main manuscript)

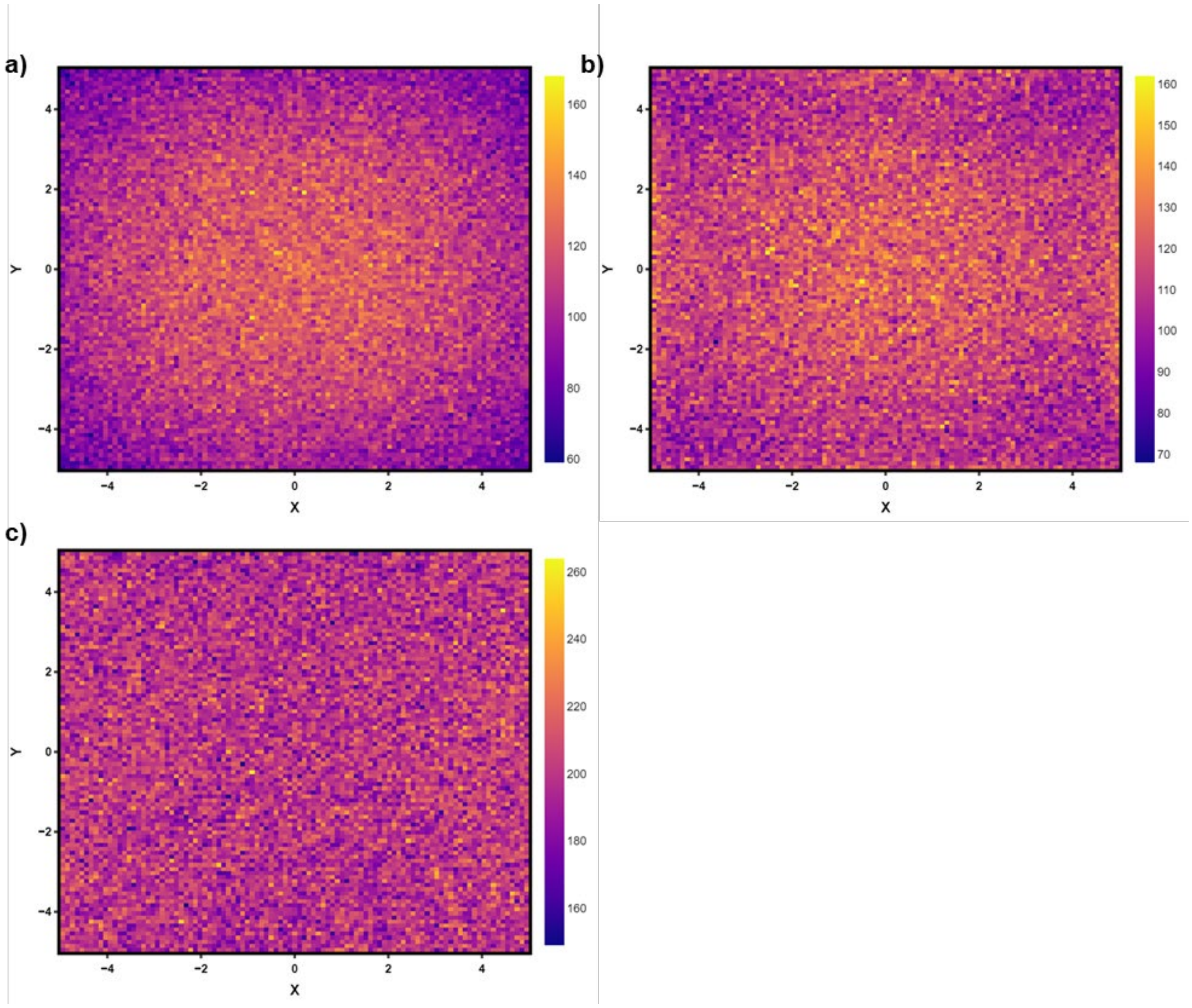

Figure 20: 2D histogram of ray hits on a flat surface. The lighting setup was 49 LEDS in an offset grid pattern with a pattern width of 12.5 cm and a light height of 5 cm. a) no diffusers or mirrors, b) diffuser at 4.75 cm above the surface. c) mirror box with a 1 cm offset from lights.

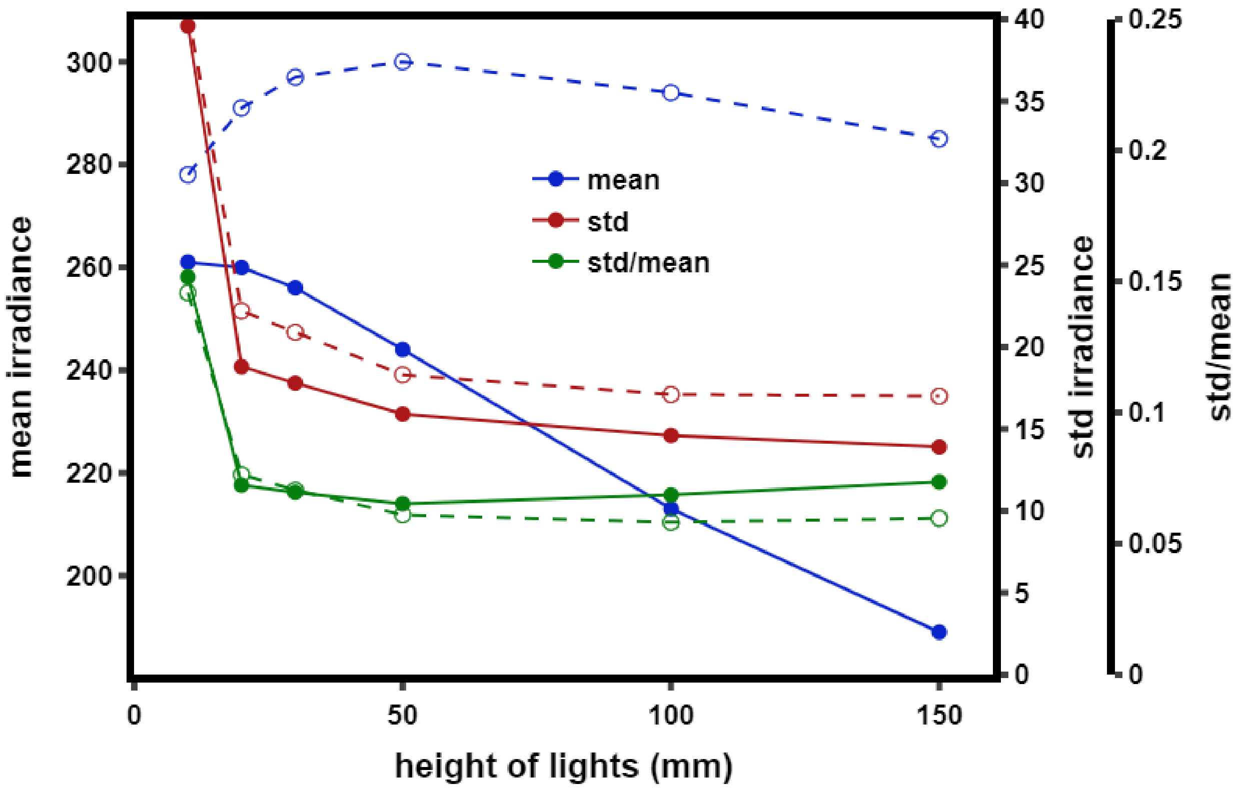

Figure 21: Dependence of mean and std of irradiance on the height of lights for mirrors with 85% (filled circles and solid lines) and 100 % (open circles and dashed lines) reflecting efficiency. The lights were in an offset grid pattern with a width of 125 mm and mirror offset of 2.5 mm illuminating a 100 x 100 mm surface.*

* The increase and decrease in mean irradiance for the 100% efficient mirror case is due to the lights pattern having width of 125 mm and the mirrors being place just outside of that. So there is a gap between the edge of the surface (100 mm square) and the mirrors where light is lost.

GIRD PATTERNS

There were four light grid patterns explored in this study: concentric circles (circle), spiral, grid, offset grid (ogrid).

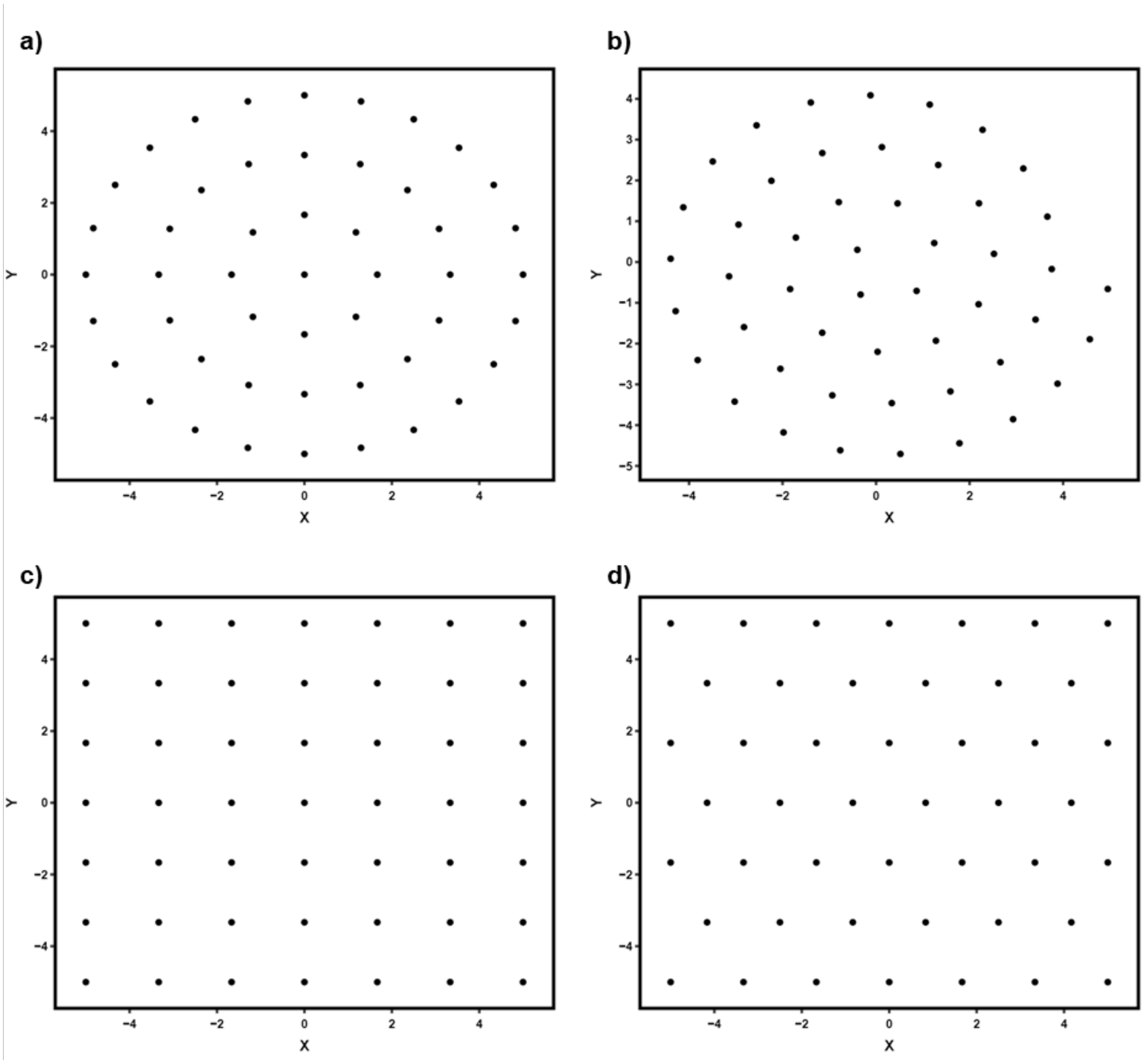

Figure 22: Examples of the grid patterns for 49 lights (the offset grid was rounded down 46 lights as that completes the pattern). a) circle pattern. b) spiral pattern. c) grid pattern. d) offset grid pattern.

EMISSION AND TRANSMITTANCE PROFILES

The led emission profile is from the DS144 LUXEON C Color Line Product Datasheet (version 20210124) from Lumileds Holding.

Data for the ground glass emission profile was from ThorLabs DG10-220-MD, Ground Glass Diffusers. Data obtained from manufacturer's website (Jan. 1, 2022). https://www.thorlabs.com/NewGroupPage9_PF.cfm?Guide=10&Category_ID=220&ObjectGroup_ID=4780

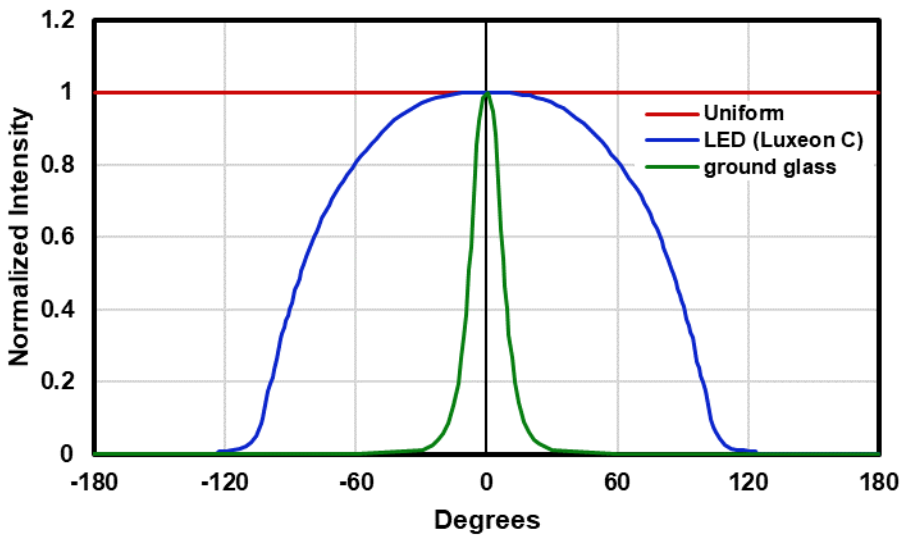

Figure 23: Emission profiles for a uniform light source, LED, and light through ground glass.

Data for transmittance through a typical ground glass diffuser was obtained from:
Ching-Cherng Sun, Wei-Ting Chien, Ivan Moreno, Chih-To Hsieh, Mo-Cha Lin, Shu-Li Hsiao, and Xuan-Hao Lee, "Calculating model of light transmission efficiency of diffusers attached to a lighting cavity," Opt. Express 18, 6137-6148 (2010) DOI: 10.1364/OE.18.006137.

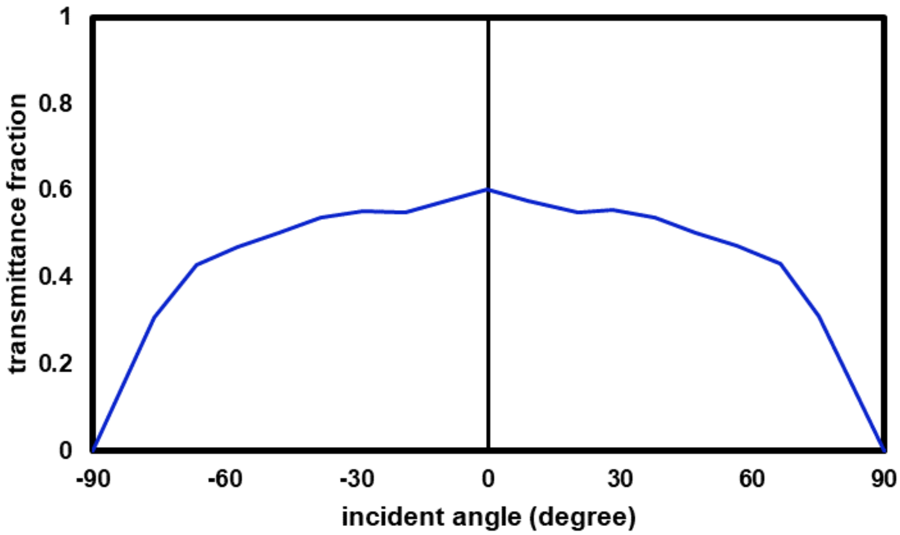

Figure 24: Transmission profile through ground glass.

ADDITIONAL PLATFORM BUILD DETAILS

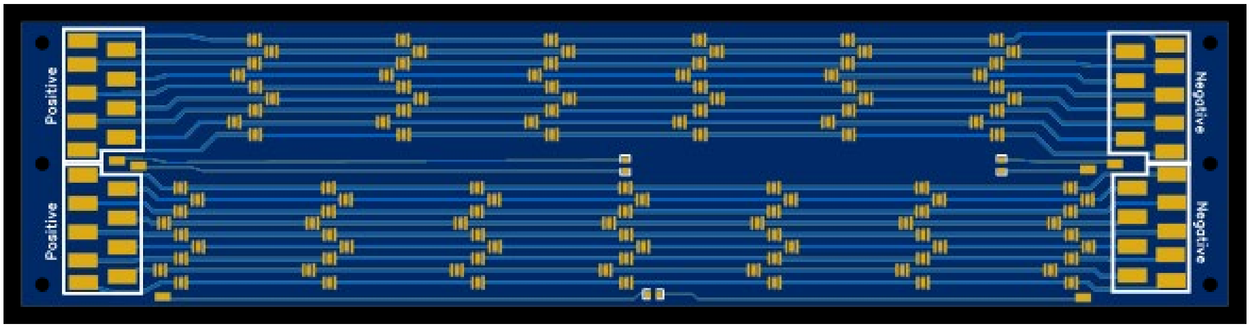

Figure 25: Design of the custom aluminum PCB for the Luxeon C Color Line LEDs.

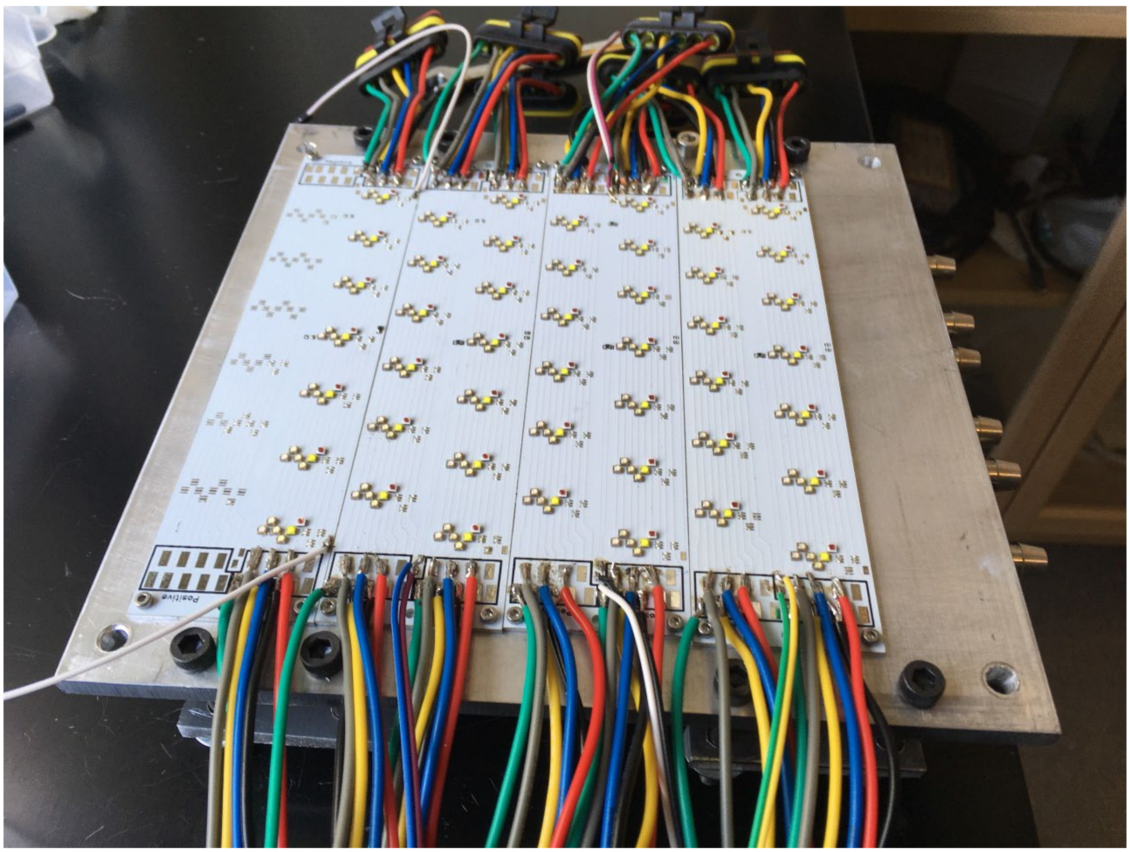

Figure 26: Photograph of complete LED assembly.

Table 1: Parts list for photochemical platform.

Part	Vendor	Vendor #	Quantity
Raspberry pi pico	Digi-key	SC0915	1
PicoBuck LED Driver	Sparkfun	COM-13705	15
High Power LEDs - Single Color Violet	Mouser electronics	L1C1-VLT1000000000	46
High Power LEDs - Single Color Blue	Mouser electronics	L1C1-BLU1000000000	46
High Power LEDs - Single Color Cyan	Mouser electronics	L1C1-CYN1000000000	46
High Power LEDs - Single Color Green	Mouser electronics	L1C1-GRN1000000000	46
High Power LEDs - Single Color Mint	Mouser electronics	L1C1-MNT1000000000	46
High Power LEDs - Single Color Deep Red	Mouser electronics	L1C1-DRD1000000000	46
THERMISTOR NTC 10KOHM	Digi-key	445-2554-1-ND	5
Mean Well 36V, 10 Amps DC power supply	Amazon		2
Clyxgs Aluminum Water Cooling Block	Amazon		3
Aluminum plate (8 in x 8 in x 0.25 in)	Mcmaster carr	9246K11	1
2020 Aluminum Extrusion, 48 in	Amazon		10
2020 Series Aluminum Profile Connector Set, 20pcs Corner Bracket, 40pcs T Nuts and Hex Screw Bolt for Slot 6mm	Amazon		2

PHOTOGRAPHS OF ILLUMINATION

To experimentally evaluate the performance of the light setup, we initially visualized the intensity and uniformity of the system with the use of a back illuminated projector screen placed in front of the lights to act as a scattering surface suitable for photographic imaging. The benefit of this approach is it is relatively simple and inexpensive to perform and has the potential for a high-resolution result. However, this technique is challenged by the screen not being a perfect scatterer and being semi-transparent. Thus, to get an accurate image, the camera must be positioned at a high angle to avoid the penetrating rays biasing the results (Figure 27). The high angle of the image makes it difficult to analyze quantitatively, but using this technique can provide a fast and qualitative analysis. Evaluating the system without mirrors with the lights and the projector screen distance of 10 cm reveals a single large hot spot, a smooth 2d gaussian-like distribution (Figure 28). On the other hand, when mirrors are added to the experimental setup a uniform illumination profile is observed supporting the simulation results.

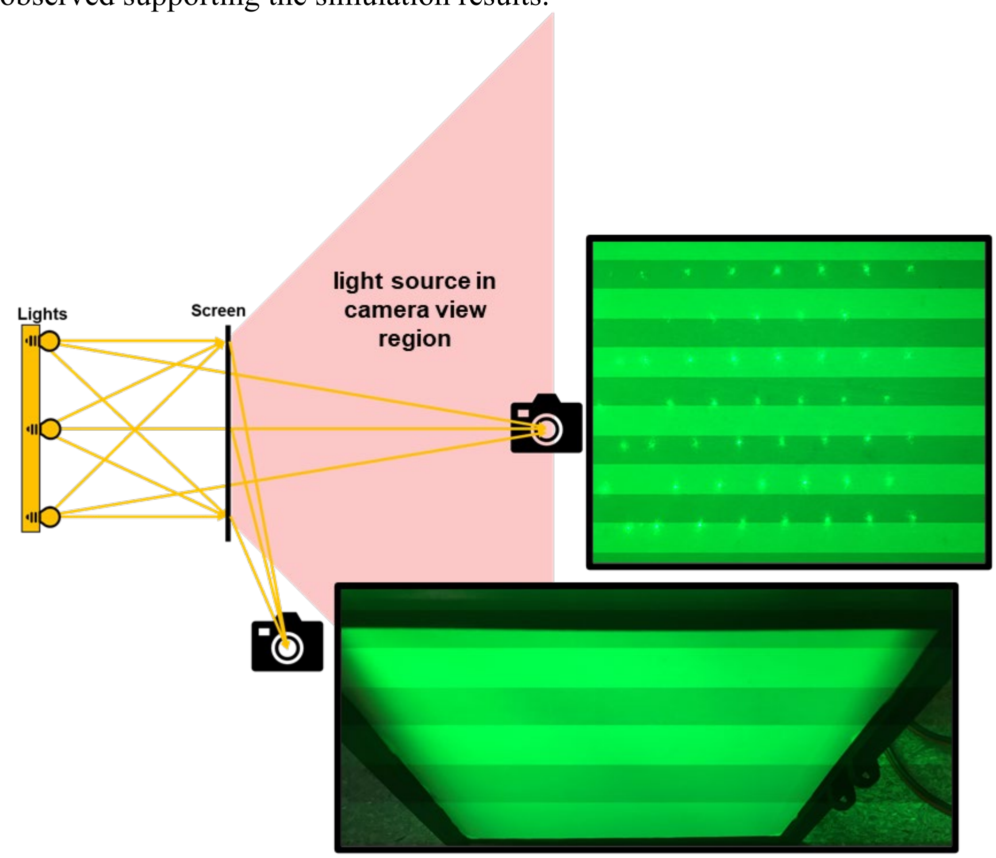

Figure 27: Diagram demonstrating the effect of camera position on the photographs.*

* See explanation on next page.

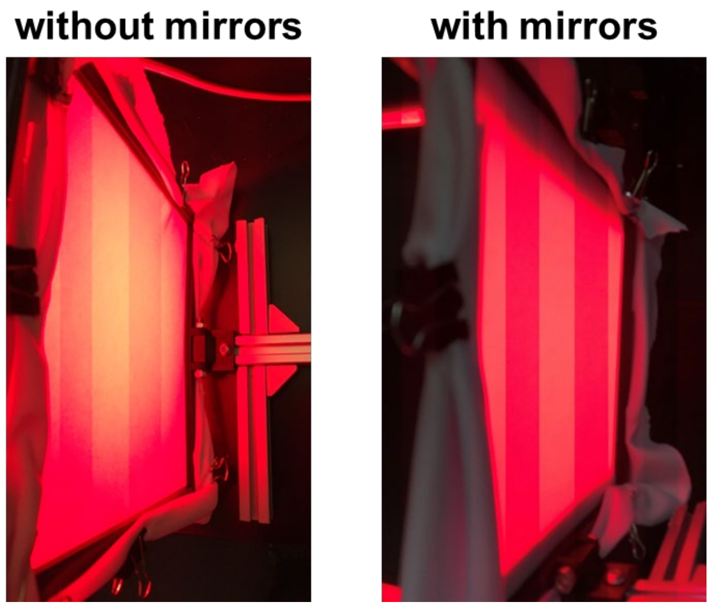

Figure 28: Photographs of the light setup with and without mirrors. The project screen is placed 10 cm away from the LED array.*

* The banding of light and dark is a result of the fact that the camera we are using scans from top to bottom, and the LEDs are set to a low dim setting (to reduce over saturating the camera sensor). Dimming on LEDs is done by turning them on-off the LED at a high frequency which on several on-off cycles occur during the exposure time of these photographs.

RADIOMETRY

The spectrometer was attached to a custom computer-controlled x-y stage to enable the collection of a heatmap of light intensity.

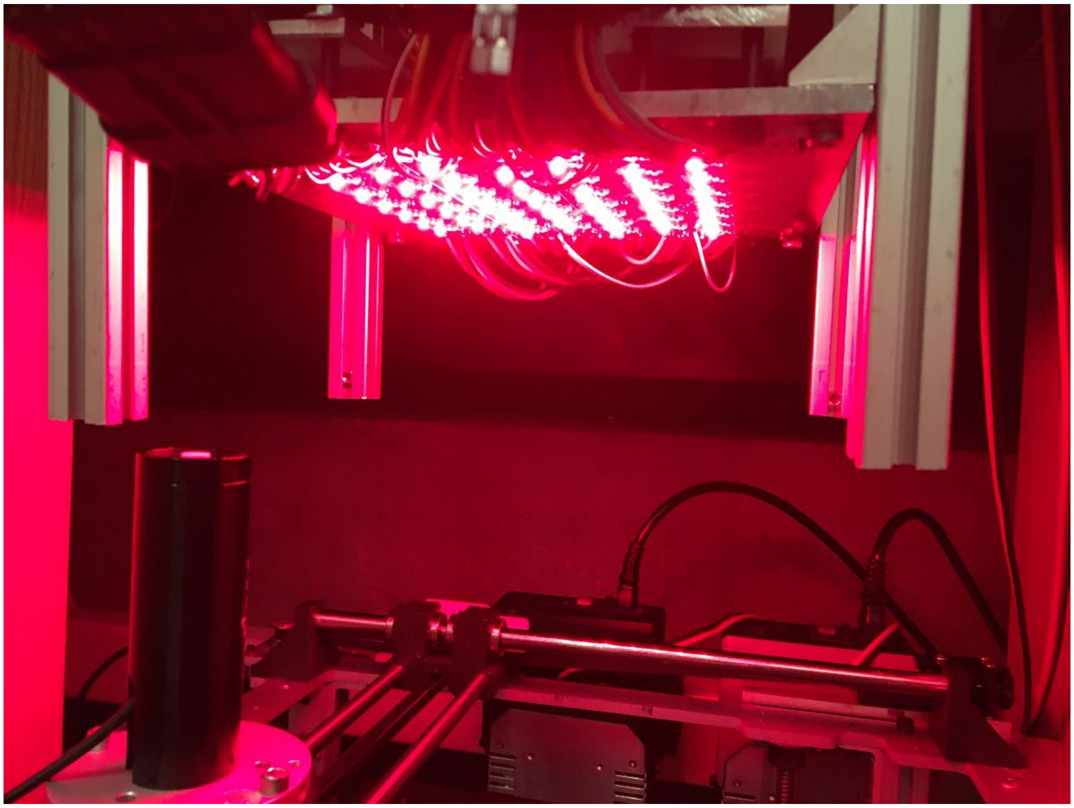

Figure 29: Photograph of the radiometry setup used to generate a heatmap.

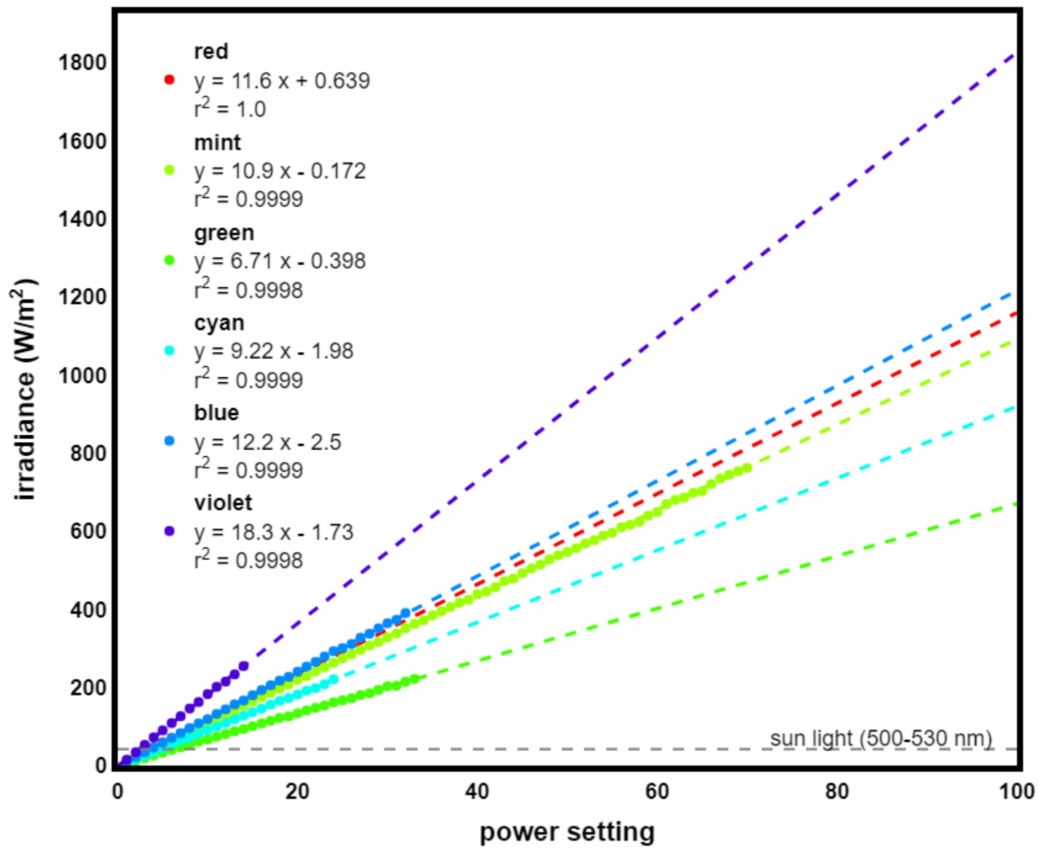

Figure 30: Irradiance vs power setting for all 6 LED colors. Measurements were taken at 80 mm below the light setup with mirrors. Data points were taken starting at the lowest power setting and increasing until the detector reached its max irradiance limit. Linear fits were applied to the data collected and projected to the max power setting.

POLYMERIZATIONS

PET-RAFT in 384 well plate with mirrors (experiment 1)

The following experiment was performed to evaluate the photo-platforms uniformity of irradiance with the photo-RAFT polymerization.

Procedure:

The polymerizations were performed by making a solution of 2-(((butylthio)carbonothioyl)thio)propanoic acid (BTPA) (48.5 mg, 0.2 mmol, 1 equiv.), zinc tetraphenylporphine (ZnTPP) (2.76 mg, 4.1 µmol, 0.02 equiv.), methyl acrylate (3.5 g, 40.7 mmol, 200 equiv.), and 3 ml of DMSO. The solution was then distributed into several wells (75 µL each) of a clear polypropylene 384 well plate. The well plate was covered and placed in the center of the light setup and exposed to green light (523 nm, 134 W/m^2, 20 % setting) for 10 min. The polymerizations were analyzed by SEC analysis by dissolving 20 µL of the reaction mixture in 1.5 ml of THF. The well plate was exposed to green light (523 nm, 134 W/m^2, 20 % setting) for another 5 minutes, and a few cells were analyzed again by SEC.

Reaction was adopted from literature.[9]

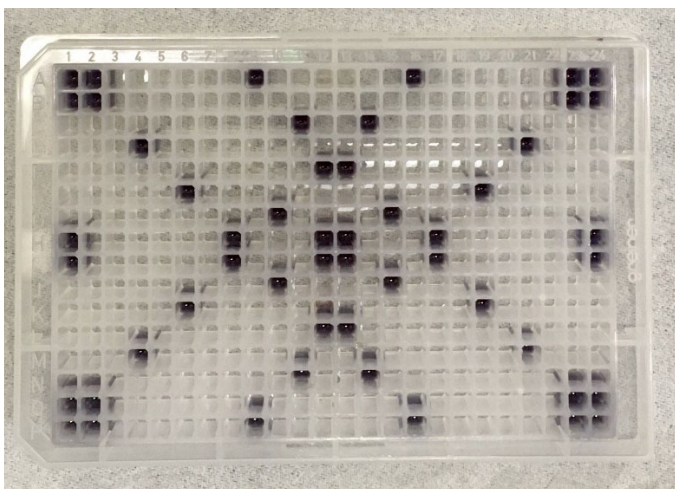

Figure 31: Photograph of well plate post-polymerization.

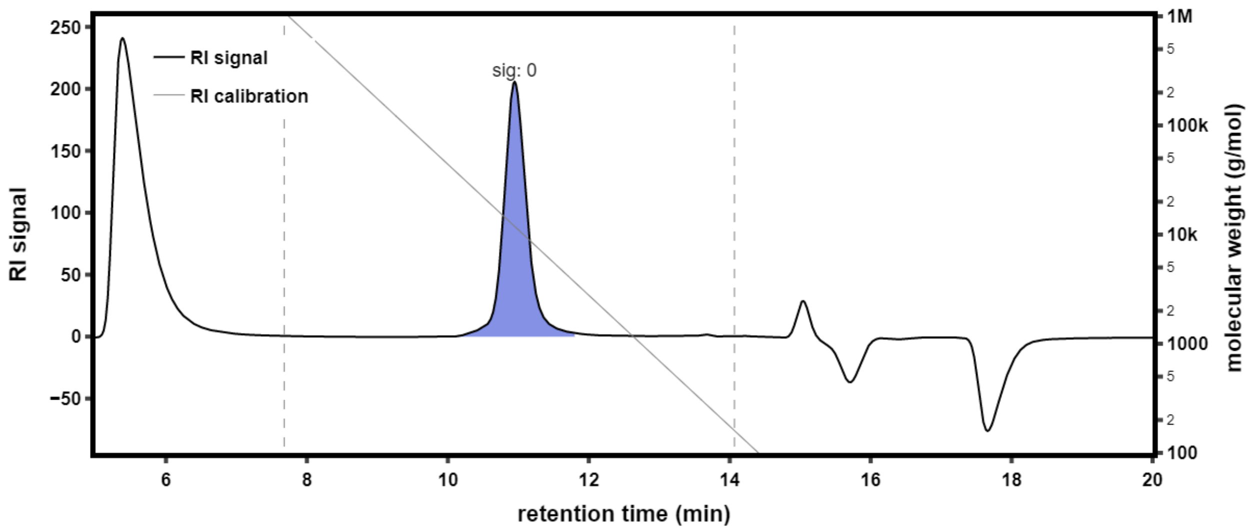

Figure 32: Representative SEC chromatogram at 10 min (showing refractive index signal for well O23). The color area under the peak indicates the area integration.*

*Overlaping injections are done. The large peak at 5 min is DMSO from the prior injection. The signals at +15 is air bubble.

Table 2: Data from the SEC analysis of PET-RAFT in 384 well plate with mirrors at 10 min.[a]

Well ID	M_n (g/mol)	Đ
A1	11,350	1.11
A2	10,780	1.09
A9	10,670	1.09
A16	10,530	1.09
A23	10,870	1.12
A24	10,900	1.12
B1	11,050	1.12
B2	10,690	1.10
B23	11,120	1.11
B24	10,890	1.12
C11	10,700	1.09
C14	10,760	1.09
D4	10,720	1.11
D21	10,740	1.10
E12	10,730	1.09
E13	10,890	1.09
F6	11,190	1.11
F19	10,760	1.09
G10	10,740	1.09
The table continues on the next page.		

G15	10,880	1.12
H1	11,130	1.12
H8	10,920	1.10
H12	10,820	1.10
H13	10,930	1.12
H17	11,310	1.11
H24	11,370	1.11
I1	10,760	1.09
I8	10,680	1.10
I12	10,870	1.10
I13	11,140	1.09
I17	10,580	1.09
I24	10,920	1.09
J10	11,170	1.11
J15	11,260	1.12
K6	11,220	1.09
K19	11,100	1.09
L12	10,970	1.10
L13	10,910	1.09
M4	11,400	1.11
M21	10,990	1.09
N11	11,440	1.11
N14	11,230	1.10
O1	11,260	1.09
O2	11,410	1.11
O23	11,000	1.09
O24	10,930	1.09
P1	11,400	1.11
P2	10,970	1.09
P9	11,430	1.11
P16	11,210	1.10
P23	11,250	1.09
P24	11,420	1.11
min	10,526	1.09
mean	11,006	1.10
std	253	0.01
max	11,445	1.12

[a] molecular weight is calculated with conventional calibration with respect to polystyrene standards.

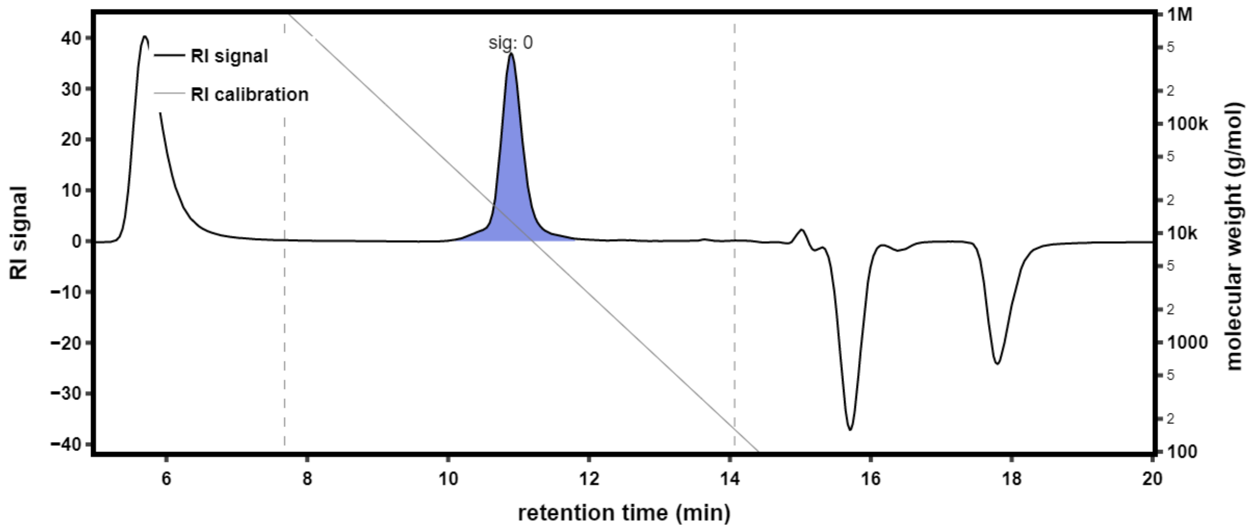

Figure 33: Refractive index SEC chromatogram at 15 min for well O23. The color area under the peak indicates the area integration.
(M_n: 12,700 g/mol, Đ: 1.11)

PET-RAFT in 384 well plate with mirrors (experiment 2)

The following experiment was performed to evaluate the photo-platforms uniformity of irradiance with the photo-RAFT polymerization and to test the reproducibility with experiment 1.

Procedure:
The polymerizations were performed by making a solution of 2-(((butylthio)carbonothioyl)thio)propanoic acid (BTPA) (48.5 mg, 0.2 mmol, 1 equiv.), zinc tetraphenylporphine (ZnTPP) (2.76 mg, 4.1 µmol, 0.02 equiv.), methyl acrylate (3.5 g, 40.7 mmol, 200 equiv.), and 3 ml of DMSO. The solution was then distributed into several wells (75 µL each) of a clear polypropylene 384 well plate. The well plate was covered and placed in the center of the light setup and exposed to green light (523 nm, 134 W/m^2, 20 % setting) for 15 min. The polymerizations were analyzed by SEC analysis by dissolving 20 µL of the reaction mixture in 1.5 ml of THF.

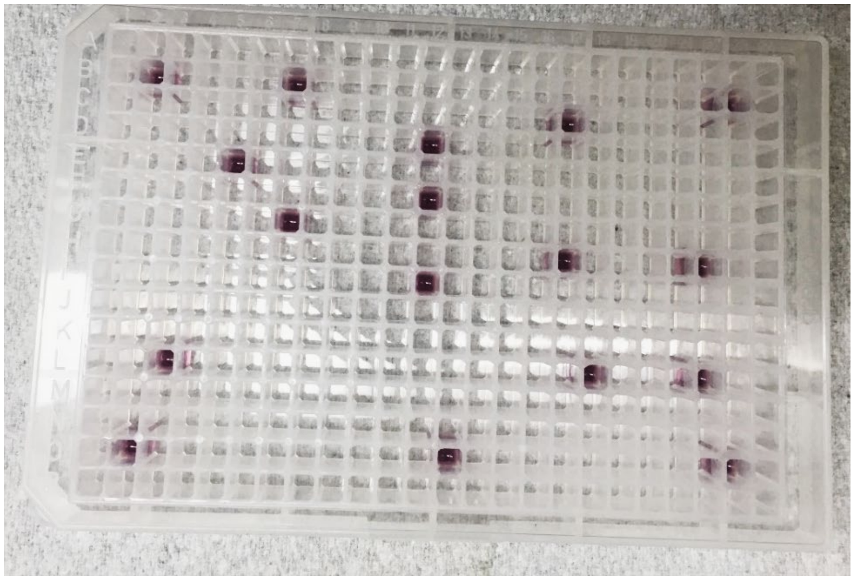

Figure 34: Photograph of well plate prior to polymerization.

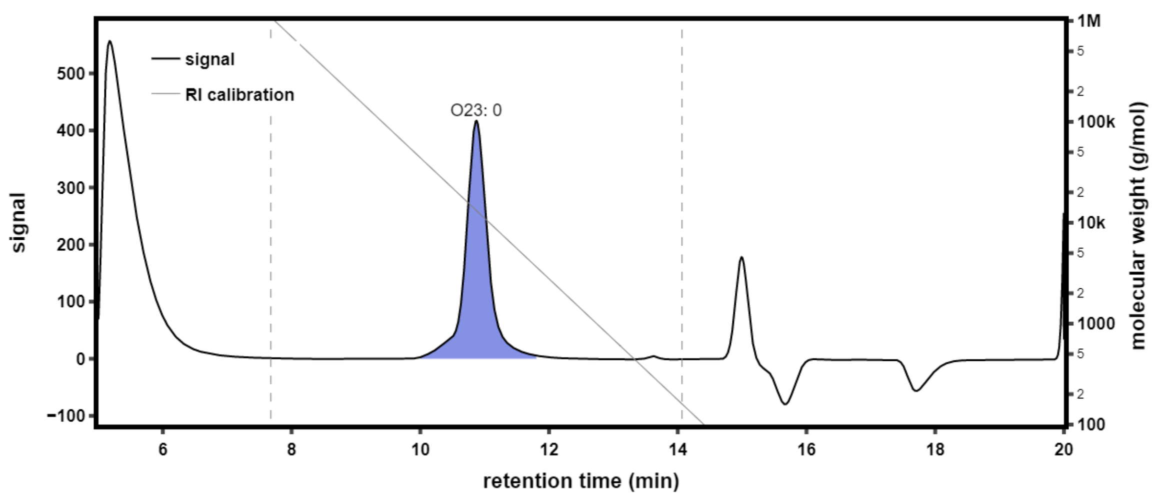

Figure 35: Refractive index SEC chromatogram at 15 min for well O23. The color area under the peak indicates the area integration.

Table 3: Data from the SEC analysis of the second run of PET-RAFT in 384 well plate with mirrors at 15 min.[a]

Well ID	M_n (g/mol)	Đ
E5	12,960	1.12
B7	12,910	1.11
D12	13,020	1.10
C17	13,040	1.11
B23	12,560	1.12
L3	12,770	1.12
I12	12,950	1.11
H22	12,860	1.11
H17	12,910	1.11
G7	12,990	1.12
F12	12,960	1.11
L18	12,970	1.12
L22	12,740	1.12
O2	12,550	1.11
O13	12,810	1.12
O23	12,540	1.11
B2	12,610	1.12
min	12,540	1.10
avg	12,832	1.11
std	170	0.004
max	13,040	1.12

[a] molecular weight is calculated with conventional calibration with respect to polystyrene standards.

PET-RAFT in 384 well plate without mirrors

The following experiment was performed to evaluate the irradiance uniformity of the photochemistry platform's without mirrors.

Procedure:

The polymerizations were performed by making a solution of 2-(((butylthio)carbonothioyl)thio)propanoic acid (BTPA) (48.5 mg, 0.2 mmol, 1 equiv.), zinc tetraphenylporphine (ZnTPP) (2.76 mg, 4.1 µmol, 0.02 equiv.), methyl acrylate (3.5 g, 40.7 mmol, 200 equiv.), and 3 ml of DMSO. The solution was then distributed into several wells (75 µL each) of a clear polypropylene 384 well plate. The well plate was covered and placed in the center of the light setup and exposed to green light (523 nm, 134 W/m^2, 20 % setting) for 10 min. The polymerizations were analyzed by SEC analysis by dissolving 20 µL of the reaction mixture in 1.5 ml of THF.

Table 4: Data from the SEC analysis of the RAFT polymerization without mirrors (at 10 min).[a]

Well ID	M_n (g/mol)	Đ
A12	5,200	1.09
B12	5,770	1.08
C12	5,940	1.08
D12	6,020	1.08
E12	6,120	1.08
F12	6,170	1.08
J12	5,920	1.09
K12	5,910	1.09
L12	5,810	1.09
M12	5,740	1.09
N12	5,850	1.09
O12	5,300	1.09
P12	4,790	1.09
H1	4,560	1.09
H2	5,630	1.09
H3	5,730	1.09
H4	5,880	1.09
H5	5,930	1.09
H6	5,990	1.09
H7	6,000	1.09
H8	6,000	1.09
H9	6,280	1.09
H10	6,020	1.09
H14	5,950	1.09
H15	6,060	1.09
H16	6,130	1.09
H17	6,170	1.09
H18	6,180	1.09
H19	6,150	1.09
H20	6,140	1.09
H21	6,090	1.09
H22	6,050	1.09
H23	5,630	1.09
H24	5,330	1.09
A1	5,050	1.09
A24	5,250	1.09
P1	4,800	1.09
P24	5,270	1.09

The table continues on the next page.

min	4,560	1.08
mean	5,740	1.09
std	470	0.003
max	6,280	1.09
[a] molecular weight is calculated with conventional calibration with respect to polystyrene standards.		

Synthesis of homo-diblock polymer by PET-RAFT in 384 well plate.

The following experiment was performed to evaluate the retention of the trithiocarbonate end-group as the high light intensity can create a higher concentration of radicals and thus a higher likelihood of termination or side reactions.

Procedure:
The polymerizations were performed by making a solution of 2-(((butylthio)carbonothioyl)thio)propanoic acid (BTPA) (48.5 mg, 0.2 mmol, 1 equiv.), zinc tetraphenylporphine (ZnTPP) (2.76 mg, 4.1 µmol, 0.02 equiv.), methyl acrylate (3.5 g, 40.7 mmol, 200 equiv.), and 3 ml of DMSO. The solution was then distributed into several wells (75 µL each) of a clear polypropylene 384 well plate. The well plate was covered and placed in the center of the light setup and exposed to green light (523 nm, 134 W/m^2, 20 % setting) for 12 min. The polymerizations were analyzed by SEC analysis by dissolving 20 µL of the reaction mixture in 1.5 ml of THF (block 1). An additional dose of methyl acrylate (37.7 mg, 0.44 mmol, 200 equiv.) in 0.38 µl of DMSO was added to the reaction and exposed to green light (523 nm, 134 W/m^2, 20 % setting) for an additional 12 min.

Table 5: Data from the SEC analysis of the homo-diblock synthesis.[a]

Polymer	M_n (g/mol)	Đ
Block 1	11,700	1.08
Di-block	22,400	1.12
[a] molecular weight is calculated with conventional calibration with respect to polystyrene standards.		

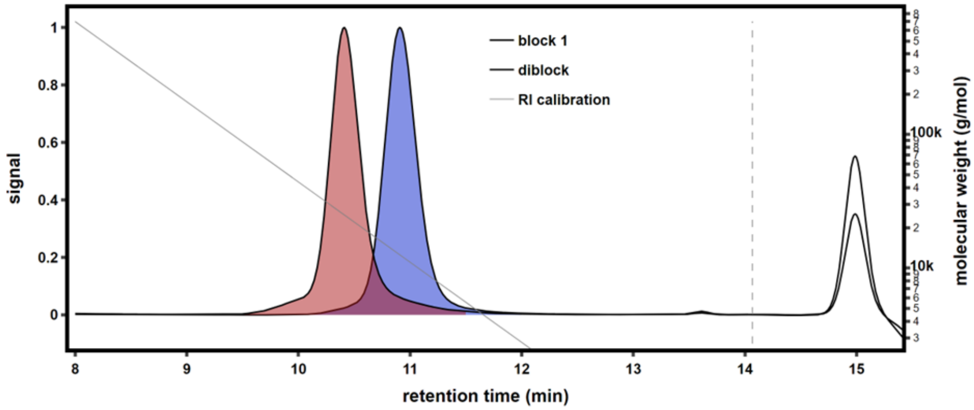

Figure 36: Refractive index SEC chromatogram for block 1 and diblock polymer. The color area under the peak indicates the area integration.

PET-RAFT in droplet continuous-flow reactor

The following experiment was performed to demonstrate versatility of the photo-platform with different experimental setups and to illustrate the reproducibility of PET-RAFT in flow.

Procedure:

The polymerizations were performed by making a solution of 2-(((butylthio)carbonothioyl)thio)propanoic acid (BTPA) (48.5 mg, 0.2 mmol, 1 equiv.), zinc tetraphenylporphine (ZnTPP) (2.76 mg, 4.1 µmol, 0.02 equiv.), methyl acrylate (3.5 g, 40.7 mmol, 200 equiv.), and 37.2 ml of DMSO. Part of the solution was withdrawn into a 10 ml glass syringe and placed in a syringe pump. A second 10 ml glass syringe was filled with N_2 and placed in a syringe pump. The two pumps were set to a flow rate of 50 µL/min (10 min residence time) each and the system was run until a steady state droplet size was reached. The reactor then was exposed to green light (523 nm, 134 W/m^2, 20 % setting). The droplets of polymerizations were taken every 2 minutes for 10 minutes and were analyzed by SEC analysis by dissolving the reaction mixture in 1.5 ml of THF.

Table 6: Data from the SEC analysis of PET-RAFT polymerization in droplet flow.[a]

Sample	M_n	Đ
1	8,180	1.07
2	8,230	1.07
3	8,180	1.08
4	8,230	1.07
5	8,080	1.07
min	8,080	1.07
mean	8,180	1.07
std	60	0.005
max	8,230	1.08
[a] molecular weight is calculated with conventional calibration with respect to polystyrene standards.		

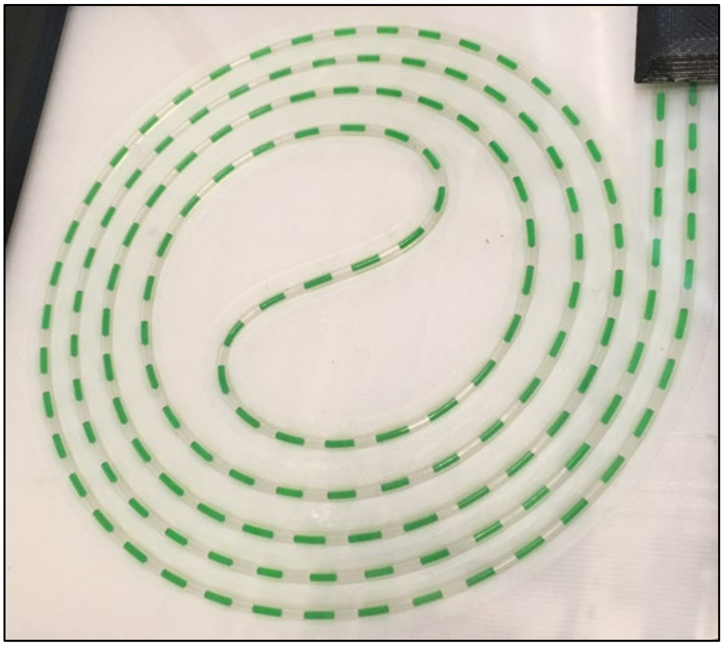

Figure 37: Image of droplet flow system between DMSO/green food coloring and air that is representative of the droplets created in the both the continuous and stop-flow droplet polymerization experiments.

PET-RAFT in droplet stop-flow reactor

The following experiment was performed to demonstrate versatility of the photo-platform with different experimental setups and to evaluate the photo-platforms uniformity of irradiance.

Procedure:

The polymerizations were performed by making a solution of 2-(((butylthio)carbonothioyl)thio)propanoic acid (BTPA) (48.5 mg, 0.2 mmol, 1 equiv.), zinc tetraphenylporphine (ZnTPP) (2.76 mg, 4.1 µmol, 0.02 equiv.), methyl acrylate (3.5 g, 40.7 mmol, 200 equiv.), and 37.2 ml of DMSO. Part of the solution was withdrawn into a 10 ml glass syringe and placed in a syringe pump. A second 10 ml glass syringe was filled with N_2 and placed in a syringe pump. The two pumps were set to a flow rate of 50 uL/min (10 min residence time) each and the system was run until a steady state droplet size was reached. The system was stopped and the N_2 syringe was vented to atmosphere to stop the droplets in place. With stationary drops, the reactor then was exposed to green light (523 nm, 134 W/m^2, 20 % setting) for 10 min. After 10 min, the light was turned off, and the drops were slowly pushed out of the reactor and were analyzed by SEC analysis by dissolving the reaction mixture in 1.5 ml of THF.

Table 7: Data from the SEC analysis of the droplet stop flow polymerization.[a]

Sample	M_n	Đ
1	8,080	1.07
2	7,940	1.08
3	7,760	1.08
4	7,900	1.06
5	8,190	1.09
6	7,790	1.07
7	7,900	1.08
8	7,660	1.05
9	8,000	1.08
10	8,100	1.07
min	7,660	1.05
mean	7,930	1.07
std	160	0.01
max	8,190	1.09

[a] molecular weight is calculated with conventional calibration with respect to polystyrene standards.

PET-RAFT in droplet flow reactor with varying light intensity (air)

The following experiment was performed to demonstrate how the photo-platform can be used for kinetic based experiments.

Procedure:

The polymerizations were performed by making a solution of 2-(((butylthio)carbonothioyl)thio)propanoic acid (BTPA) (48.5 mg, 0.2 mmol, 1 equiv.), zinc tetraphenylporphine (ZnTPP) (2.76 mg, 4.1 µmol, 0.02 equiv.), methyl acrylate (3.5 g, 40.7 mmol, 200 equiv.), and 37.2 ml of DMSO. Part of the solution was withdrawn into a 10 ml glass syringe and placed in a syringe pump. A second 10 ml glass syringe was filled with air and placed in a syringe pump. The two pumps were set to a flow rate of 50 uL/min (10 min residence time) each and the system was run until a steady state droplet size was reached. The reactor then was exposed to green light (523 nm) at different power amounts (power setting: 2, 5, 10, 20, 30, 40, 60, 100; watts: 13.2, 33.4, 66.9, 134, 201, 268, 402, 670 W/m^2). The droplets of polymerizations were analyzed by SEC analysis by dissolving the reaction mixture in 1.5 ml of THF.

No reaction was observed at 2 and 5 power settings. This is likely due the known induction period of the polymerization, while the photocatalyst is reacting with oxygen.[10]

Table 8: Data from the SEC analysis of the homo-diblock synthesis.[a]

Power setting	Irradiance (W/m^2)	M_n (g/mol)	Đ
10	67	3,560	1.21
20	134	6,110	1.18
30	201	7,400	1.18
40	268	8,020	1.23
60	402	9,130	1.28
100	671	8,650	1.52
[a] molecular weight is calculated with conventional calibration with respect to polystyrene standards.			

The broader molecular weights distributions and lower M_n were due to the use of air, instead of N_2. At higher light intensity, side/termination reaction led to an increase in molecular weight dispersity.

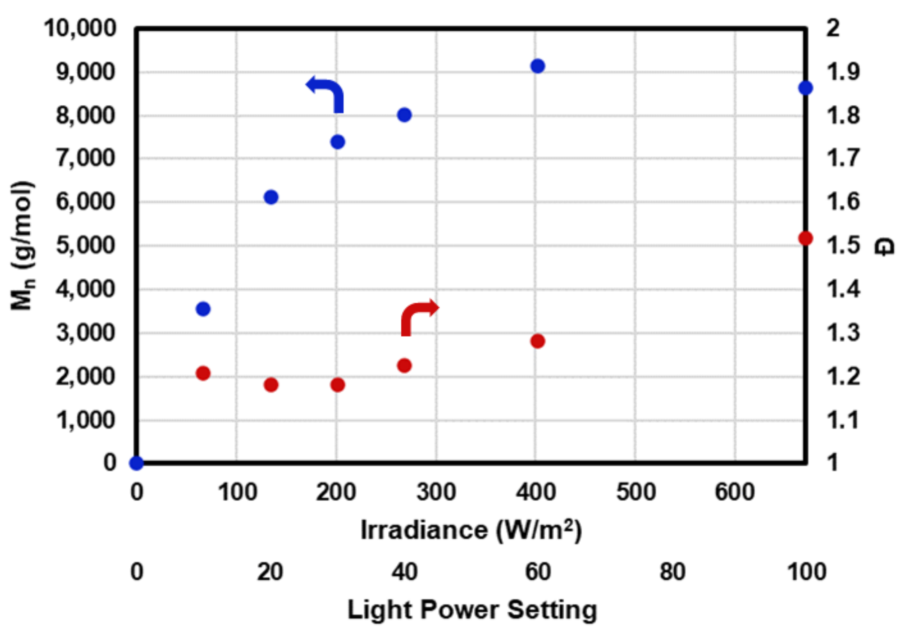

Figure 38: The change in M_n and Đ with respect to varying irradiance for the droplet flow (10 min residence time) PET-RAFT polymerization.

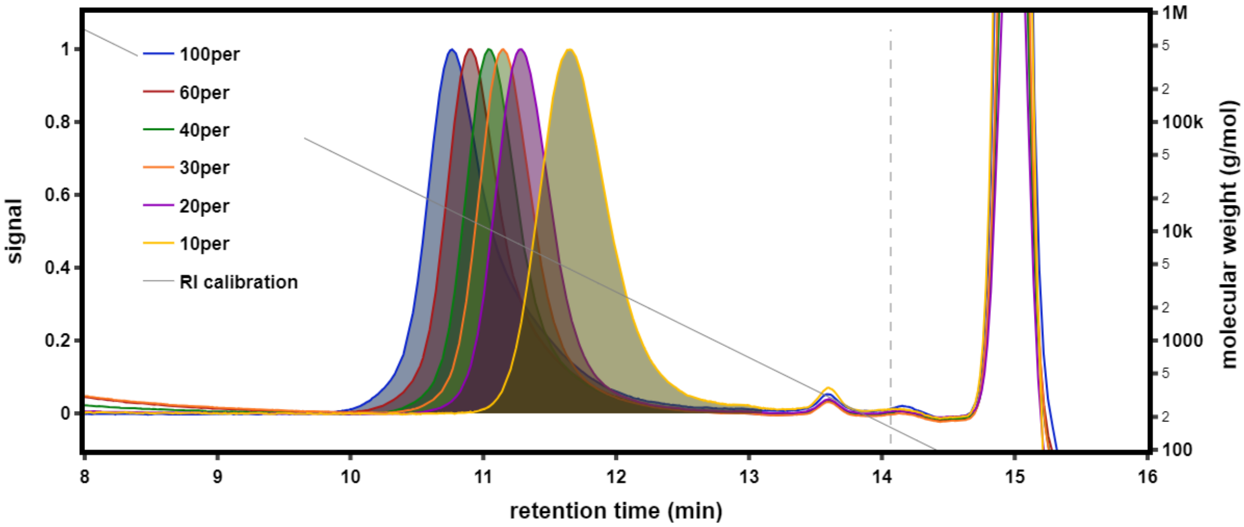

Figure 39: Refractive index SEC chromatogram for PET-RAFT polymerization in droplet flow with varying intensities of light. 'per' in the legend is short for light 'power setting percentage'. The color area under the peak indicates the area integration.

ANALYTICAL EQUIPMENT

Size Exclusion Chromatography (SEC) was performed using a Tosoh Ecosec HLC-8420GPC at 40 ºC with THF (HPLC grade) as the eluent. This SEC is equipped with both a refractive index and UV detector. The SEC is fitted with a guard column (TSKgel Guard SuperH-H 4.6 mm ID x 3.5 cm, 4 µm), and two analytical columns (TSKgel SuperHM-M 6 mm ID x 15 cm, 3 µm) and reference column (TSKgel SuperH-RC 6 mm ID x 15 cm, 4 µm). The reference flow rate is 0.45 mL/min while the analytical column is at 0.45 mL/min. Polystyrene standards (16 points ranging from 160 g/mol MW to 1.1 million g/mol MW) were used as the general calibration.

$$MW = 10^{0.601\,time(min)+10.644}$$

Black-Comet C-25 Spectrometer purchased from StellarNet with a measurement range 190-850nm outfitted with an Apogee cosine corrected radiometric head. The instrument was calibrated by Apogee (serial number: 21042742).

REFERENCE

(1) Smith, W. J. *Modern Optical Engineering*, 4th ed.; McGraw Hill Professional, 2007.

(2) Ryer, A. D. The Light Measurement Handbook; International Light Technologies, 1997.

(3) Sun, C.-C.; Chien, W.-T.; Moreno, I.; Hsieh, C.-T.; Lin, M.-C.; Hsiao, S.-L.; Lee, X.-H. Calculating Model of Light Transmission Efficiency of Diffusers Attached to a Lighting Cavity. *Opt Express* **2010**, *18* (6), 6137. https://doi.org/10.1364/OE.18.006137.

(4) Moreno, I.; Contreras, U. Color Distribution from Multicolor LED Arrays. *Opt Express* **2007**, *15* (6), 3607. https://doi.org/10.1364/OE.15.003607.

(5) Moreno, I.; Sun, C.-C. Modeling the Radiation Pattern of LEDs. *Opt Express* **2008**, *16* (3), 1808. https://doi.org/10.1364/OE.16.001808.

(6) Jacobs, V.; Forment, S.; Rombauts, P.; Hanselaer, P. Near-Field and Far-Field Goniophotometry of Narrow-Beam LED Arrays. *Lighting Research & Technology* **2015**, *47* (4), 470–482. https://doi.org/10.1177/1477153514530139.

(7) Photonics Media. *Mirrors: Coating Choice Makes a Difference*. https://www.photonics.com/Articles/Mirrors_Coating_Choice_Makes_a_Difference/a25501 (accessed 2022-06-04).

(8) Weisstein, E. W. Sphere Point Picking. *https://mathworld.wolfram.com/SpherePointPicking.html*. MathWorld--A Wolfram Web Resource.

(9) Shanmugam, S.; Xu, J.; Boyer, C. Exploiting Metalloporphyrins for Selective Living Radical Polymerization Tunable over Visible Wavelengths. *J Am Chem Soc* **2015**, *137* (28), 9174–9185. https://doi.org/10.1021/JACS.5B05274.

(10) Xu, J.; Jung, K.; Atme, A.; Shanmugam, S.; Boyer, C. A Robust and Versatile Photoinduced Living Polymerization of Conjugated and Unconjugated Monomers and Its Oxygen Tolerance. *J Am Chem Soc* **2014**, *136* (14), 5508–5519. https://doi.org/10.1021/ja501745g.